2011

Effects of a Heated Turbulent Boundary Layer on Surface Pressure Fluctuations

David William Rich

Effects of a Heated Turbulent Boundary Layer on Fluctuating Surface Pressures

David W. Rich

A thesis submitted in partial fulfillment
of the requirements for the degree of

Masters of Science
Engineering Science
Aeroacoustics

University of Mississippi

May 2011

Abstract

Recent work has shown that spatial correlation of surface pressure fluctuations in a fully turbulent atmospheric boundary layer (ABL) can give information about the velocity field and turbulence. This is of particular importance to the future of wind energy to predict the incoming velocity flow field of wind turbines so as to actively control them for peak operating efficiency and damage reduction. All of the environmental effects on the surface pressure fluctuations need to be fully understood before a suitable flow prediction algorithm can be constructed. One such environmental effect which has not been previously studied is the effect of surface heating on the surface pressure fluctuations.

The current study aims to create a situation in a low speed wind tunnel that is roughly analogous to that of a ground heated turbulent ABL and to study the effects on the surface pressure fluctuations. The intent was not to perfectly scale the ABL but to create a situation in the wind tunnel that mimics some of the same physical processes associated with the ABL.

Experimental data was collected in the $2' \times 2'$ square test section low speed wind tunnel at the University of Mississippi's National Center for Physical Acoustics. A 3" tall backward facing step was placed at the entrance of the test section to create a sufficiently thick, fully developed turbulent boundary layer further down the test section where surface pressure fluctuations were measured. The bottom floor of the

tunnel was also retrofitted with electric heater blankets so as to study the effect of surface heating on the surface pressure fluctuations.

The effect of heating on surface pressure fluctuations was studied for a variety of flow speeds and surface temperatures and it was shown that the surface heating had little to no effect on any of the measurements of the sound pressure level beneath the boundary layer. It was also shown from the cross-correlation coefficient functions that the surface heating had little to no effect on the calculated turbulent convection speeds.

Acknowledgments

I would like to thank Nathan Murray for encouraging me to pursue a graduate degree, for acceptance into the aeroacoustics program, and for all of his guidance and advice with my academic career and this thesis. I would also like to thank Bernie Jansen for all of his help in the lab, setting up the actual experiment, and being an invaluable resource for any technical question imaginable. I would like to thank Praveen Panickar for all his help with the programming required to run the experiment and his help with the data analysis after the experiment. The funding for this project was provided by the United States Department of Energy under agreement DE-EE0003269. I would also like to thank my family for their loving support and thank God for all His many blessings in my life.

Table of Contents

List of Figures

List of Tables

Chapter 1

Introduction

With the ever increasing energy demands of the United States there is also an increased interest in diversifying the energy production portfolio. Fossil fuels such as coal and natural gas, which at present constitute about 65% of our total electric power generation, have only a limited supply. The greatest shift in energy production will be toward renewable energy sources such as solar energy and wind energy. The United States Department of Energy (DOE), in a landmark report made in 2008, stated goals for the electrical energy production future of the United States. In this report, the DOE stated a goal of 20% of the total electrical energy production in the United States come from wind energy by the year 2030. To put into perspective how drastic of a shift this would be in energy policy, wind energy currently only constitutes about 2% of the total electrical energy production in the U.S.

The reason wind energy only constitutes 2% of the U.S. electrical energy production is because it currently is cost prohibitive. For the most part, the areas of the country that are geographically suitable for wind energy production do not have very dense populations. Since the population in the areas of most wind farms is sparse, great cost is associated with the subsequent electrical power transmission infrastructure required to supply more densely populated areas. Another reason wind energy

is not as cost effective as other energy sources is that large tracts of land are required for wind farms. Perhaps the greatest limiting factor in the future of wind energy is the current technology of wind turbines.

Because the cost of large scale wind turbines is so high, the reliability and durability of the components as well as the operating efficiency are paramount. Turbulence in the incoming velocity field causes unsteady blade loading which results in component fatigue and ultimately destruction if not compensated for. Large unpredictable wind gusts can also cause the turbine to rotate too quickly and damage components. Even if the incoming velocity field were relatively stable to an upwind turbine, the downstream turbines in its wake will likely see unsteady inflow conditions. If a non-intrusive method could determine the incoming velocity field and turbulence in real time this information could be used to dynamically control the operation of the wind turbine and its components.

One such proposed method is to use arrays of ground based pressure transducers to measure surface pressure fluctuations to gain insight on the incoming flow field. This is possible because when a turbulent flow moves over a surface, the hydrodynamic forces convecting with the flow can be measured as surface pressure fluctuations. Because the atmospheric boundary layer is generally analogous to that of a turbulent flat plate boundary layer the same situation exists. For a ground based pressure transducer system to be successfully implemented as part of a control sequence for wind turbines, a much broader understanding of the problem must be gained. The goal of this experiment is to simply study one component of the broader problem associated with using surface pressure fluctuation measurement to predict flow characteristics. The effect of surface heating on the surface pressure fluctuations and their correlations with flow velocity in a turbulent boundary layer are to be studied

in a wind tunnel so as to gain possible insight on some of the phenomena that may exist in full scale atmospheric conditions.

1.1 Boundary Layer Theory

The earliest work in theoretical fluid mechanics was based upon the principal of the ideal fluid. An ideal fluid is thought of as one that is inviscid and incompressible. In inviscid fluids there exists no shear stresses between adjacent layers in the fluid or other walls. However, real fluids are not inviscid and because of this there exists tangential shear or frictional forces between layers in the fluid and the fluid with solid boundaries. For ideal fluids the fluid velocity at a solid boundary is different than the velocity of the boundary and therefore the fluid slips alongs the boundary. However for real fluids a no-slip condition exists between a fluid and a solid boundary and therefore a frictional force and shear stress also exist at the boundary. Newton was the first to note that the shear stress can be related to the velocity gradient with the relation

$$\tau = \mu \frac{\partial u}{\partial y} \tag{1.1}$$

where τ is the shear stress, $\partial u/\partial y$ is the gradient of the velocity and μ is the fluid's dynamic viscosity. Reynolds (1883) was the first to note that flows could be thought of as mechanically similar if they exhibited the same ratio of inertial forces to viscous forces. The dimensionless Reynolds number is given below as

$$Re = VL_c/\nu \tag{1.2}$$

where V is the flow velocity, L_c is some characteristic length scale associated with the flow, and ν is the kinematic viscosity. The kinematic viscosity is related to the

dynamic viscosity as $\nu = \mu/\rho$. Prandtl (1904) was the first to introduce the concept of boundary layer flow. The concept was based on the idea that for flow over and around surfaces there existed a thin boundary layer where all viscous flow effects were confined. For regions of the flow outside of this boundary layer the viscous effects were thought to be negligible. Inside of the boundary layer the velocity of the fluid is affected by the shearing resistance of the boundary due to the no-slip condition. Prandtl gave a qualitative description of boundary layer flow and also simplified the Navier-Stokes equations to be applied to boundary layer flows. Blasius (1908), one of Prandtl's students, obtained exact numerical solutions to Prandtl's equations for large Reynold's number laminar boundary layer flows over flat plates.

One of the most common examples of boundary layer theory is flow over a thin, smooth flat plate. An example of this type of flow can be seen in Fig 1.1. As a uniform flow field approaches the plate and intersects the plate, the fluid far away from the plate continues to move at its original free stream velocity but the fluid at the plate's surface will be stationary due to the no-slip condition. For this reason a velocity gradient exists between the fluid in the free stream and the fluid at the plate surface. A shear stress exists at the surface of the plate due to the vertical velocity gradient as was shown in Eq 1.1. The shear stress at the surface of the plate retards the fluid particles near the plate and they decelerate as they move downstream over the plate. Since these particles are now at a lower velocity than those above them a shear stress exists between them which will slow the higher altitude particles as they move downstream. The boundary layer grows in the downstream direction due to the existence of shear stress between more and more fluid particle layers. The boundary layer thickness, the point at which the velocity is 99 % of the free stream velocity U_∞, will be denoted as δ.

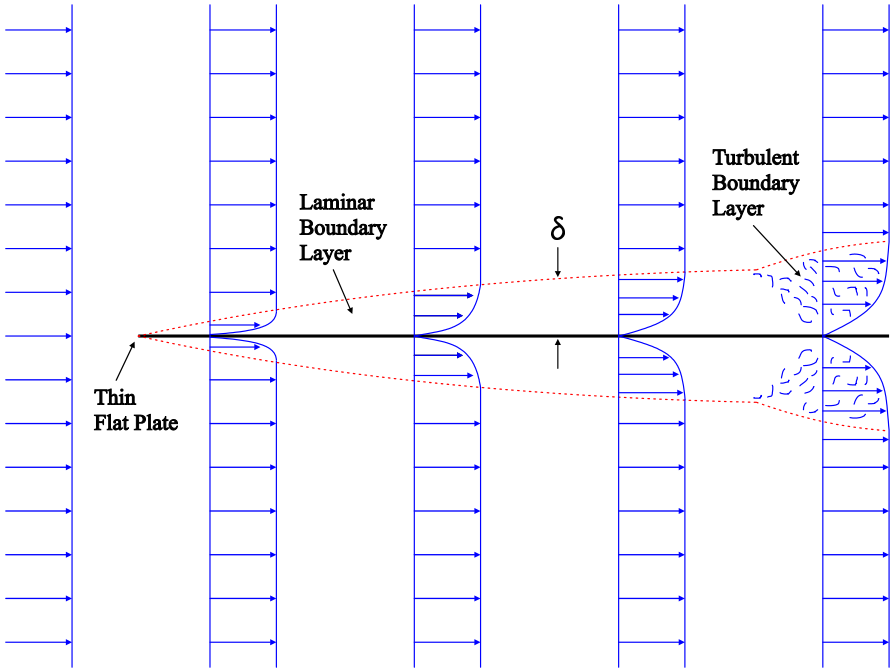

Figure 1.1. Development of a boundary layer over a thin flat plate.

The thickening of the boundary layer will continue downstream until a point is reached where the flow becomes unstable and turbulence exists in the boundary layer. The critical Reynold's number, based on the downstream distance from the leading edge of the plate, at which the boundary layer transitions to turbulence is generally accepted to be $Re_{crit} \approx 5 \times 10^5$. In laminar boundary layers the viscous effects are present in the entire boundary layer and the flow field can be solved for from Blasius' solutions. However, for turbulent boundary layers the flow field is more complex and requires more than one model to solve for the different regions of the flow field. In turbulent boundary layers the flow is usually broken up into three different regions: the inner layer, the outer layer, and the overlap layer. In the inner layer the viscous shear effects are dominant where as in the outer layer turbulent eddy shear effects are dominant. In the overlap region both types of shear are important.

In the inner, or viscous sublayer, the velocity distribution is related to the shear stress and viscosity by Eq 1.1. A common term used in non-dimensional analysis of boundary layer flows is the friction velocity u^*. The friction velocity is related to the shear stress at the wall τ_w and the fluid density ρ as

$$u^* = \sqrt{\tau_w/\rho} \tag{1.3}$$

Two more non-dimensional variables will now be introduced as $u^+ = u/u^*$ and $y^+ = yu^*/\nu$. For the viscous sublayer the velocity profile is linear and this non-dimensional velocity profile can be given as $u^+ = y^+$. The viscous sublayer is very, very thin, usually at least two orders of magnitude smaller than the overall boundary layer thickness. Because the viscous sublayer is so thin, experimentally measuring it has traditionally been difficult.

The outer region of a turbulent boundary layer can be approximated by the use

of the log-law. The log-law is given in Eq 1.4 where K and C are constants. Typical values of K and C that are widely used and determined by Coles & Hirst (1968) are 0.41 and 5.0 respectively, but other values are sometimes used that are close to these. The log-law is valid for values of y^+ from about 30 to 500. Prandtl's mixing-length theory is to be thanked for the development of the log-law shown as Eq 1.4 (Prandtl, 1925).

$$u^+ = \frac{1}{K} \ln y^+ + C \tag{1.4}$$

The log-law is not the only velocity profile estimation used for turbulent boundary layers; there also exists the power law. The power law was first introduced by Barenblatt *et al.* (1997) and it provides an estimation for velocity profiles of turbulent boundary layers for flat plate flow as well as pipe flow. The general power law is shown as Eq 1.5

$$u^+ = C(y^+)^\alpha \tag{1.5}$$

where C and α are constants that will vary with Reynolds number. The power law also takes the more familiar form of Eq 1.6.

$$\frac{u}{U_\infty} = (\frac{y}{\delta})^{1/7} \tag{1.6}$$

1.2 ABL Applications to Wind Turbines

The present study aims to make some observations on the effect of surface heating in a turbulent boundary layer on pressure fluctuations measured at the surface. The ultimate end goal is that the findings of this study will give insight into phenomena that may exist in turbulent atmospheric boundary layers so surface pressure fluctu-

ation measurements can be used to dynamically control wind turbines for optimum performance. A brief description of flat plate turbulent boundary layers was given in the previous section but their relationship to atmospheric boundary layers needs to be discussed further.

As complex as flat plate turbulent boundary layers are, atmospheric boundary layers are even moreso. Atmospheric boundary layers also have the added variability of surface heating and cooling, air humidity, and the earth's rotation. The turbulence of atmospheric boundary layers also differs from the turbulence that can usually be studied in wind tunnels. The turbulence in a wind tunnel is usually strictly mechanically generated turbulence, that is it results from shear effects. In atmospheric boundary layers thermal convection interacts with mechanical turbulence and creates a more complex system.

The basic structure of ABL's does show similarity to two-dimensional turbulent boundary layers that are created in wind tunnels. ABL's generally have two different regions, an inner and outer, and under neutrally stable conditions ABL's will have a velocity profile that can be approximated by the log-law or the power law. Most wind turbines are designed with neutral stability as the basis which is rather surprising because neutral stability conditions only exist for two brief periods each day (Sim *et al.*, 2009). Neutral stability conditions occur in transitional periods such as sunrise, or sunset, or even under daytime cloud cover where buoyancy effects on the air are absent. While most wind turbines were designed with neutral stability conditions in mind, the ABL is usually very stable at night or very unstable during daylight hours.

Negative buoyancy is created at night when the ground cools rapidly and is at a lower temperature than the air in the free stream above it. The lower temperature air at lower altitudes cools the warmer air at higher altitudes causing it to become

denser and sink toward the ground. These negative buoyancy effects act to damp out turbulence created by wind shear. During stable ABL conditions the vertical velocity gradient is much higher and wind shear is greater.

During the daytime, when cloud cover is minimal, the ground heats up from solar radiation. The ground below becomes much warmer than the air above it. The ground heats the layer of air immediately above it causing it to become less dense. This warmer air rises and cooler air takes it place which is again heated by the ground and the process repeats itself. As the warm air rises vertically and interacts with the wind flowing normal to it, vortical structures are created which convect downstream. During the unstable ABL conditions the vertical velocity gradient at the surface is lower than for unstable conditions so wind shear is not as detrimental to turbines. However, the turbulence is much greater and gusts can severely damage turbines.

It is easily seen through boundary layer theory that flow velocity increases with increasing distance from the boundary. Glauert (1934) showed that the theoretical maximum power that could be extracted from a wind turbine was given as Eq 1.7. In Eq 1.7 A denotes the swept area of the turbine blades and can be given as $A = \pi r^2$ where r is the blade length. Since the power extracted from the wind increases with the cube of the wind velocity and the square of the blade length, it is easy to see why wind turbines are built as high as possible with the longest blades possible.

$$P_{max} = \frac{16}{27}\left(\frac{1}{2}\rho U^3 A\right) \tag{1.7}$$

Creating taller wind turbines with longer blades seems like a simple idea but creates a myriad of engineering difficulties. With increasing height and velocity inflow also comes increased torque on the blades. Engineers want to create the lightest blades possible that will allow the turbines to begin spinning and generating power

at low wind speeds. The blades also need to be stiff enough to withstand extreme loading in high wind speeds. Unfortunately, as turbine blades are being built larger, they are also becoming more flexible. All of the problems associated with turbulence are exacerbated in large wind turbines where the blades are more dynamically active due to their increased flexibility and are thus more susceptible to fatigue loading and failure.

A main contributor to wind turbine failure is uneven blade loading due to shear forces. It was shown previously that the velocity in the boundary layer increased with height. During nightime conditions, where the velocity gradients in the vicinity of turbines is greatest, very large turbines with rotor diameters of 70 meters and greater can be subjected to much lower wind velocities at the bottom of the rotor and much higher wind velocities at the top of the rotor. Because of this velocity gradient, as the rotor spins the individual blades are constantly subjected to changing loads. The highest load occurs when the blade is at its highest position and the lowest load occurs when the blade is at its lowest position. Coherent turbulent structures also exist at nightime and the short bursts of adverse loading conditions caused by them is probably more destructive than vertical wind shear across the rotor (Kelley *et al.*, 2005).

During the daytime unstable ABL there exists vortical structures formed from the interaction of buoyantly convected air from the surface with wind blowing parallel to the surface. There also exists mechanical turbulence associated with wind shear. The interaction of turbulent vortical structures on wind turbines can also be very damaging and the prediction of them is very difficult. Measurements of the wind profile with ground based pressure transducers has been proposed but the effect of the surface heating on this process is one aspect that needs to be studied further.

1.3 Surface Pressure Fluctuations

There are currently two main types of active measurement systems that are employed to measure wind profiles incoming to wind turbines: LIDAR or Light Detection and Ranging and SODAR or Sonic Detection and Ranging. LIDAR shines a beam of coherent UV light, a laser, vertically through the incoming flow field and makes wind speed measurements by detecting the shift in frequency of the light that is reflected from aerosols that are naturally present in the atmosphere. SODAR works in a similar manner to LIDAR. SODAR systems send out a pulsed sound wave and analyzes the reflected signal to gain a measurement of the wind speed and direction. While LIDAR and SODAR systems have been proven as successful measurement devices of wind speed, they do have several disadvantages. Both types of systems are only capable of giving vertical wind profiles at a single location and both types of systems are very expensive. Furthermore, SODAR is only capable of giving averaged values for wind speed, and can't give information about turbulence. For these reasons these systems are not adequate for use to measure inflow wind conditions of an entire wind farm or to make wind measurements between individual turbines.

A low cost passive system is desired that can accurately measure wind conditions around a wind farm. Arrays of ground based pressure transducers may be able to accomplish this task. Past research proves that temporal-spatial correlations between surface pressure fluctuations beneath a turbulent boundary layer can give information about the convective speed of the the flow at some elevation above them (Willmarth, 1956). Measurements of surface pressure fluctuations with multiple sensors would need to be simultaneously taken with either LIDAR, SODAR, or multiple anemometers at various heights so the actual velocity field could be related to convective speeds as determined by the temporal-spatial correlations of pressure sensors. To create a

suitable flow prediction algorithm from surface pressure fluctuation measurements, this type of experiment would need to be performed for a variety of actual inflow conditions such as strong stability, neutral stability, and instability.

The study of wall pressure fluctuations beneath turbulent boundary layers is not new; research on the subject began in the late 1950's with works from Kraichnan (1956) and Willmarth (1956). The original goal of measuring surface pressure fluctuations beneath turbulent boundary layers was to gain insight into the structure and physical mechanisms of the turbulence which produced them and also to address many engineering problems associated with them. Some of the earliest engineering problems with which surface pressure fluctuation studies could be applied included fatigue loading on structures such as aircraft, as well as problems concerning acoustic radiation from the vibration of the surface due to the fluctuating pressures (Bull, 1996). In the late 1950's and early 1960's when the preliminary research in this field began, acoustic measurement of wind profiles and detection of turbulent structures that could damage wind turbines was not even on the horizon.

Willmarth (1956) was the first to publish research dealing with the basic statistical structure of the wall pressure field beneath a turbulent boundary layer. Because this was a completely new concept, this early work dealt with the creation of a low noise and low turbulence wind tunnel in which to take measurements. This study also addressed the need to vibrationally isolate the surface mounted pressure transducers so as to not mistakenly measure wind tunnel vibrations. Willmarth took data for both laminar and turbulent boundary layers and his results showed a considerable increase in levels of the surface pressure fluctuations beneath a turbulent boundary layer as compared to a laminar one. This early study only used a single pressure transducer so only temporal correlations were possible.

Work in this field of study continued throughout the 1960s by researchers such as Bull (1967), Serafini (1963), and again Willmarth & Wooldridge (1962). The research in this period began dealing with measurements of the mean square pressure, frequency spectra, and temporal-spatial correlations of the wall pressure fluctuations. Correlations were also made of the wall pressure fluctuations to the velocity fluctuations in the boundary layer so as to gain an insight into the relationship of wall pressure patterns and coherent turbulent structures in the boundary layer. All of the researchers found that an estimate of turbulent convective speed could be made by dividing the spatial distance between two sensors by the time lag between peaks of their cross-correlation function. This was the speed at which the coherent turbulent structures of the boundary layer were transported downstream. Willmarth & Wooldridge (1962) found that the convective speed ranged from 56 - 83% of the free stream velocity and the convective speed measured increased with sensor spacing. Bull & Willis (1961) also confirmed their findings and found the turbulent convective speed ranged between 70 and 85% of free stream velocity. These researchers also noted a difficulty in minimizing sensor size so as to be relatively small compared to the boundary layer thickness.

Velocity fluctuations in all parts of the boundary layer contribute to the pressure fluctuations measured at the surface as was theorized by Lighthill (1952). Because the turbulence at various heights in a boundary layer convects downstream at different speeds due to the mean velocity profile of the boundary layer, the structure of the wall pressure field was found to be very complex. Farabee & Casarella (1991) Keith *et al.* (1992) searched for some universal scaling that would satisfy the surface pressure fluctuations for a myriad of flow conditions. These researchers never studied the effect of surface heating beneath the turbulent boundary layer and how it might

affect the surface pressure fluctuations.

The remainder of this document gives a brief description of the wind tunnel which was used for the experiment and how it was modified with a backward facing step to create a thick turbulent boundary layer. Details are also given about the construction of a heated flooring system which allowed for the effect of surface temperature on the surface pressure fluctuations to be studied. A description of the pitot-static probe system used to measure the mean velocity profiles throughout the tunnel is given as well as a description of the actual surface pressure sensors and the data acquisition system used. The results of the mean velocity profiles which were measured as well as the results of the statistical analysis of the surface pressure fluctuations are both given. A conclusions section with a summary of all the results is given as well as recommendations for future work.

Chapter 2

The Experiment: Design, Setup, & Execution

The experimental data that was used for this study was acquired in the $2' \times 2'$ test section low-speed wind tunnel facility at the University of Mississippi's National Center for Physical Acoustics. The tunnel was modified in such a way as to produce a sufficiently thick turbulent boundary layer and was retrofitted with heating elements on the bottom floor of the test section. Floor mounted pressure transducers were also mounted on the bottom floor of the tunnel to measure the surface pressure fluctuations with and without floor heating. The original attempt at using 3/32" Kulite pressure transducers flush mounted with the heating elements proved unsuccessful. 1/4" Panasonic microphones were instead used and flush mounted in a thin, smooth strip that was attached on top of the heating elements along the tunnel centerline. A traverse system was set up at the top wall of the tunnel test section which allowed a pitot-static probe to be used to measure the mean velocity profile at different locations in the test section. Section 2.1 describes the wind tunnel and its basic operating characteristics, Section 2.2 details the construction and installation of the backstep, Section 2.3 details the construction of the new heated floor, Section 2.4 details the top wall and traverse system used to obtain mean velocity profiles, and Section 2.5 details the pressure transducers.

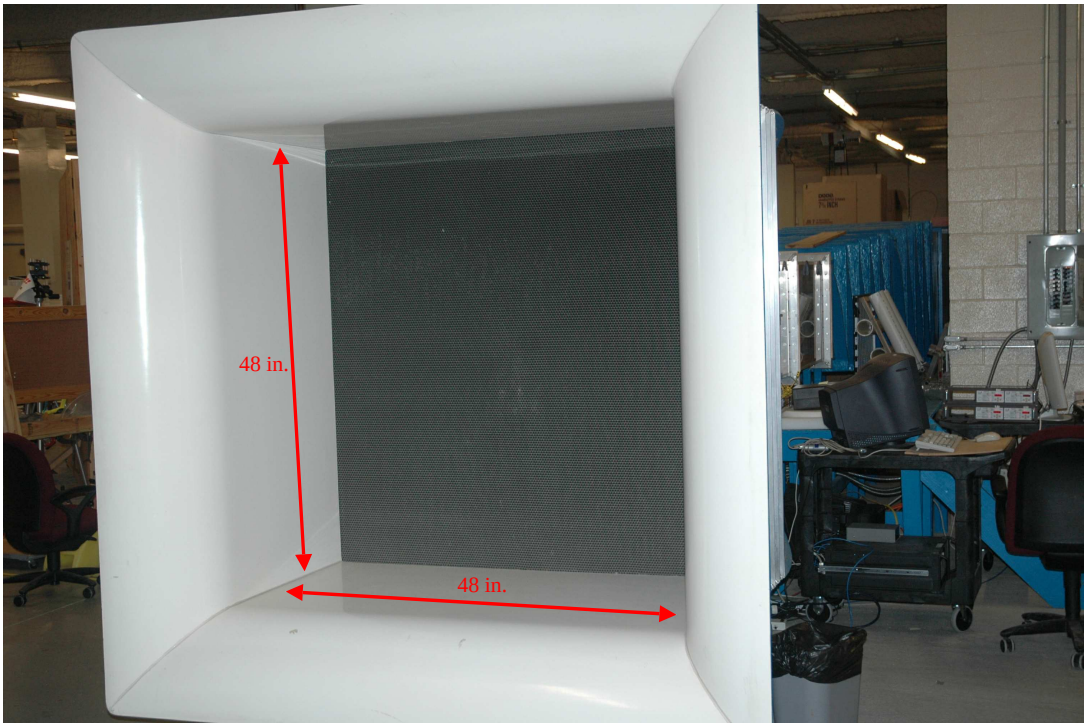

Figure 2.1. $4' \times 4'$ **Inlet section of NCPA low speed wind tunnel.**

2.1 Wind Tunnel Description

The $2' \times 2'$ low speed wind tunnel at the University of Mississippi's National Center for Physical Acoustics is an open-circuit National Physical Laboratory (NPL) type wind tunnel with a 7.5 horsepower, 3-phase, 4 pole, induction motor which is controlled with a Toshiba Transistorized Inverter. The tunnel, before modifications, is capable of free stream speeds of about 50 ft/s. The inlet section of the tunnel is $4' \times 4'$ which provides for a contraction ratio 4:1. The diffuser section of the wind tunnel is $14.5'$ long and the walls diffuse at a $4°$ angle. The inlet section of the wind tunnel is shown below in Figure 2.1.

The tunnel test section is $8'$ long and all of the walls are constructed of 3/4" thick

plexiglass. The top wall is completely removable so as to allow for the insertion of models and the side walls are fitted with removable plugs which allow for the insertion of instrumentation to measure the flow.

2.2 Backward Facing Step

A sufficiently thick fully developed turbulent boundary layer needed to be created for this experiment so pressure fluctuations on the surface beneath it could be measured. It was shown previously in Section 1.3 that the for a flat plate the flow would transition to turbulence at a $Re_L \approx 5 \times 10^5$. Since the test section had an overall length of $8'$ and could attain speeds of 50 ft/s, a turbulent boundary layer could easily be attained in the test section. The problem, however, was that the boundary layer would not be sufficiently thick to take measurements in to resolve its profile. Another reason the boundary layer needed to be thick and turbulent was that the surface pressure fluctuations were to be spatially correlated to one another to obtain a convective turbulence speed. It was already shown in Section 1.5 that there exists a relationship between the sensor spacing and the convective speed that will be observed. Because of this fact and that the sensors being used were 1/4" in diameter, a thick boundary layer was needed so multiple sensor spacings could be used to relate the pressure fluctuations to the convected velocity.

One such proposed method of creating a thick turbulent boundary layer in the wind tunnel was to place a backward facing step at the beginning of the tunnel test section. A side view of the general flow pattern over a backward facing step is shown in Figure 2.2. Considerable amounts of research have been done dealing with flow over backward facing steps such as that of Eaton & Johnston (1980), Armaly *et al.* (1983), and Adams & Johnston (1985), primarily due to its simple geometry, but also

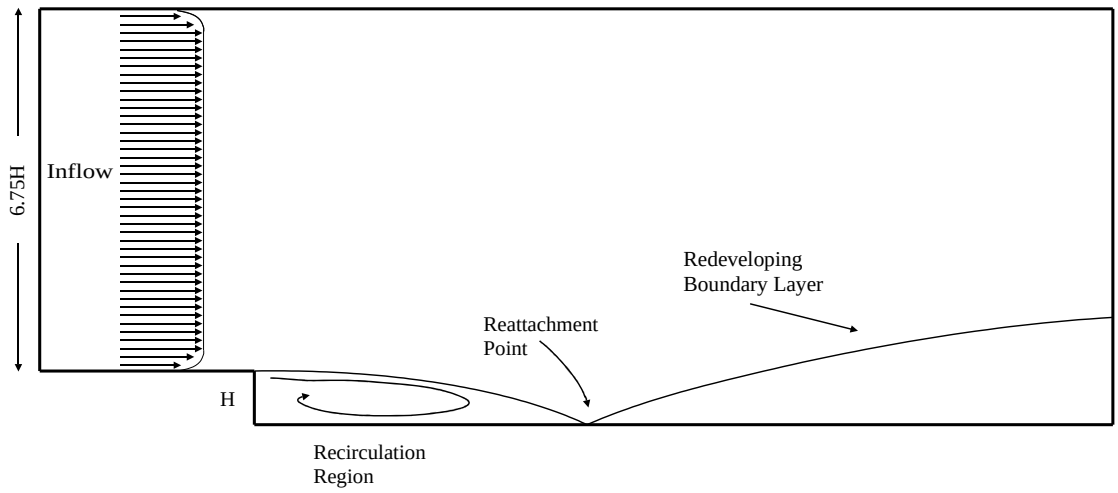

Figure 2.2. Example of flow over a backward facing step

because there are many real world scenarios where this type of flow occurs.

As the flow moves over the step a free shear layer forms from the top edge of the step. This free shear layer moves downstream and grows and eventually it grows large enough that it comes back in contact with the bottom wall surface and the flow reattaches. Between this reattachment point and the base of the step there exists a recirculation region. The distance of the point of reattachment has been studied previously by Durst & Tropea (1981) and shown that it is dependent on the expansion ratio and Re_H, where Re_H is the Reynolds number based on the height of the step. For flows over backward facing steps it has generally been agreed upon that flows below Re_H of 1200 are laminar, between 1200 and 6600 are transitional, and above 6600 are fully turbulent. The expansion ratio for duct flow over a backward facing step is defined as the ratio of the cross sectional area perpendicular to the flow before the step and after the step.

The area immediately following the reattachment point of the flow is called the

recovery region of the flow. In the recovery region the mean streamwise velocity profile of the flow does not match that of a standard turbulent boundary layer profile but redevelops and further downstream the flow again will take the standard form of a turbulent boundary layer. The boundary layers behind backward facing steps do not typically resume the shape of a normal flat plate boundary layer until at least 50 step heights downstream (Kim *et al.*, 1978). However, the boundary layer will contain coherent turbulent structures, not unlike those that are seen in a turbulent atmospheric boundary layer.

From the information gathered from this earlier work it was decided that a step height of 3" would be used for this study with a free stream velocity of 30 ft/s at the beginning of the step for a Re_H of about 50,000. When the new heated floor, to be discussed later, was placed in the tunnel this would give a distance vertical distance from the top of the step to the top wall of 20.25" and a distance from floor to top wall of 23.25". This gives an expansion ratio, ER, of 1.148.

Le *et al.* (1997) performed a direct numerical simulation of flow over a backward facing step for a transitional Re_H of 5100 and an expansion ratio of 1.20. They found that a reattachment length of $6.28H$ existed and the flow was still recovering downstream to $x/H = 19$. The expansion ratio they used was very close to this study but their Reynolds number was only transitional and not fully turbulent as was in the case with this study. Since only a 3" step height was used for this study, and the tunnel test section was 96" long, measurements could be made out to $x/H = 32$.

The backward facing step was built by using a piece of wood 3.75" $\times$ 3.75" $\times$ 24" and attaching it to the bottom floor of the tunnel using double sided carpeting tape. A 1/32" thick piece of sheet tin was attached to the top of the step and also attached to the lower surface of the tunnel contraction. The sheet metal was cut about $4'$ long

Figure 2.3. View of 3" backward facing step installed in tunnel contraction.

and allowed to extend into the contraction section and lay flat so as to follow the curve of the existing contraction. This created a smooth transition from the existing tunnel contraction section to the top of the backward facing step. The reason the step was cut to be 3.75" tall was because the new heated floor that would be installed later would be 0.75" thick. The backward facing step can be seen in Fig 2.3. The sides of the sheet metal were attached to the existing tunnel contraction using a pliable rubber tape.

2.3 Heated Floor

The goal of this project was to study the effects of surface heating on pressure fluctuations beneath a turbulent boundary layer so a method for actually heating the bottom surface needed to be created. The reason for heating the boundary layer was to hopefully be able to create some buoyant natural convection. When a surface is much warmer than its surroundings, some of the heat from the warmer surface will conduct to the air immediately around it and warm it up. As the temperature of the air immediately adjacent to the surface warms it becomes less dense than the cooler air above it. The warmer air rises from the surface and is replaced by cooler air and the process repeats itself continually.

The Grashof number is a dimensionless quantity representing the relationship between the buoyant forces and the viscous forces acting on a fluid. Grashof number is given below in Eq 2.1 where g is the acceleration due to gravity, β is the coefficient of thermal expansion, T_s is the temperature of the surface, T_∞ is the temperature of the fluid sufficiently far away from the surface, L_c is the characteristic length of the geometry, and ν is the kinematic viscosity of the fluid.

$$Gr_L = \frac{g\beta(T_s - T_\infty)L_c^3}{\nu^2} \tag{2.1}$$

Since the scenario in this study actually involves forced fluid flow over the heated surface, there will also be a forced convection of heat away from the surface. The relative importance of each form of convection, forced and natural, is given as the ratio of Gr/Re^2. If $Gr/Re^2 \gg 1$, then natural convection dominates. If $Gr/Re^2 \ll 1$, forced convection dominates. If Gr/Re^2 is $O(1)$, then both forms of convection are significant. It was hoped that a ratio of Gr/Re^2 on the order of 1 could be had for this experiment because the intersection of the fluid convecting upward from the

bottom floor and the forced flow parallel to the floor would interact and create vortical structures. If this were to occur it may be possible to detect the vortical structures as they traveled downstream with the surface pressure fluctuation measurements.

Most literature on heat transfer such as Cengel (2007) addresses mixed forced and natural convection problems such as flow over a vertical heated flat plate. For a vertical heated flat plate with fluid flowing parallel to its surface, the natural convection effects directly assist or oppose the heat transfer away from the surface. The problem is more complicated when the natural convection effects are normal to the flow over the surface. For horizontal flat plate flow the characteristic length L_c generally associated with Reynolds number is the length along the plate from the leading edge. For a heated rectangular flat plate the characteristic length associated with Grashof number is generally given as the surface area A_s divided by the perimeter p. Because a backward facing step was used in this experiment to create the boundary layer, it is uncertain what length scale to use in a comparison of the Grashof number to the Reynolds number.

The basic design for the new heated floor needed for this experiment was a three layered system of plywood, sheet metal, and electric silicone rubber coated heater pads. The plywood was used because it provided stiffness and rigidity and served as the main structural component of the flooring system. The plywood would also serve as an insulating material that would protect the existing plexiglass floor. Some type of insulation was needed between the floor heating elements and the plexiglass because plexiglass only has a maximum working temperature $150°F$ - $200°F$. A thin layer of tin sheet metal was applied on top of the plywood to give a smooth layer for the silicone rubber heaters to be attached. The tin sheet metal layer would also work to distribute the heat evenly over the entire surface of the floor. The electric silicone

rubber coated heater elements were chosen because they were available in thin flat sheets, provided high heat flux, supplied even heating over their surface, and were relatively inexpensive.

The basic construction method of the heated floor sections is shown in Fig 2.4. A piece of 1/2" thick plywood was cut $4'$ long and $2'$ wide to fit in between the existing plexiglass walls of the wind tunnel. A $2' \times 4'$ piece of sheet tin was cut and attached to the top surface of the plywood panel with a layer of red RTV silicone rubber adhesive. This type of adhesive was used because it works very well for high temperature applications and is basically the same material that is used in the heater pads. Before the sheet metal was attached to the plywood, two pockets were created on the top surface of the plywood where thermocouples could be flush mounted. The two K-type thermocouples were mounted $1'$ from each end of the plywood and 6" from either side of the plywood.

1/16" thick, $1' \times 4'$ Tempco brand electric heaters were used for this experiment. The heaters had a watt density of 5 W/in^2 which yielded a total power of 2.88 kW per heater. The heaters were built to operate on 120 VAC power which meant that each heater had an internal resistance of 5 Ω. For each floor section two of the heaters were wired together in series and supplied with 208 VAC electricity. This yielded a current of 20.8 A through the heater bundle and a total power output of 4.33 kW per pair of heaters. The total power output of the entire heated floor system was 8.66 kW. The heater wiring diagram and control circuit is shown in Fig 2.5.

To keep the floor at a relatively constant temperature, a thermostat system needed to be created. A solid state relay was used to switch power on and off to the heaters. A solid state relay is a device which basically acts as an on-off switch but has no moving contacts; this is good for a thermostat application where a large number of

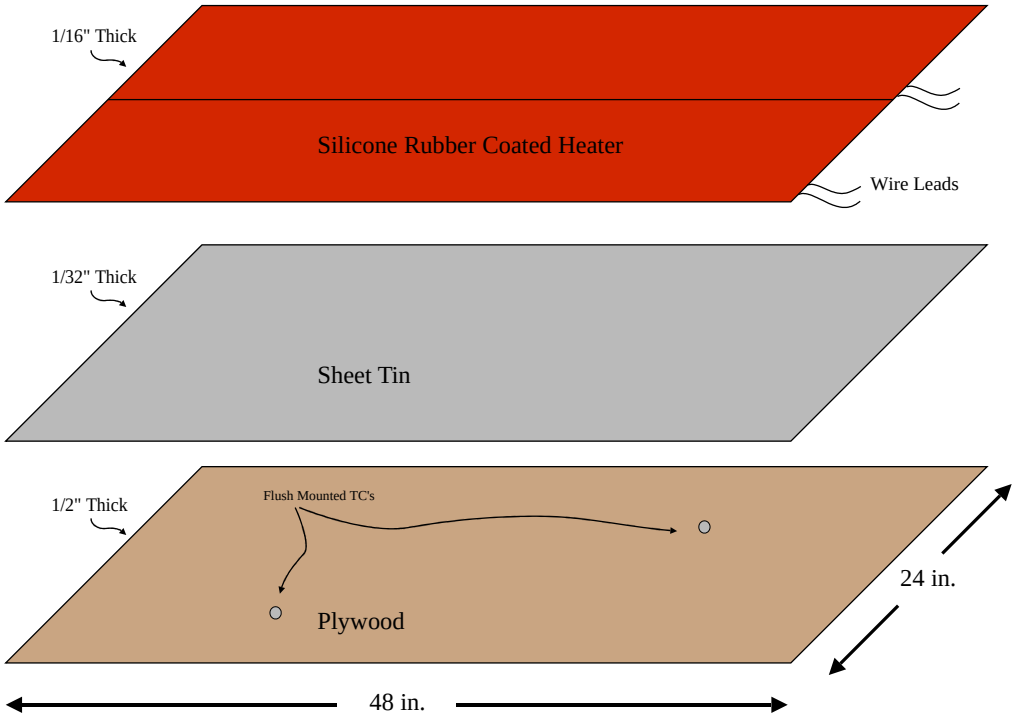

Figure 2.4. Schematic of heated floor design.

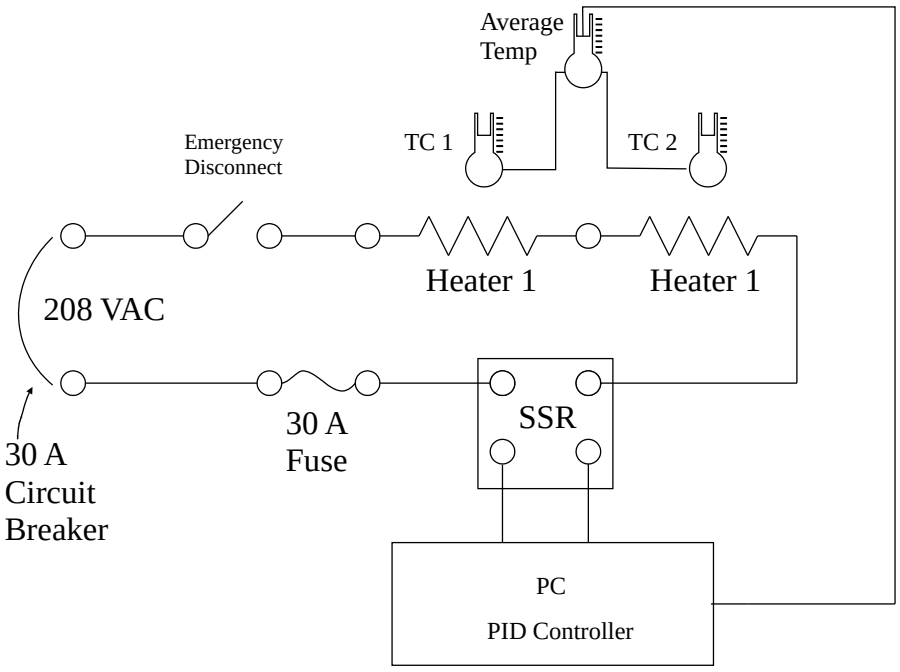

Figure 2.5. Basic floor heater wiring diagram and control circuit

cycles are required which would wear out a conventional mechanical contact switch. A control voltage is applied to the relay which is used to "open" or "close" the contacts and allow current to flow. An Omega SSRL240DC50 solid state relay was used to switch the power on or off to each pair of heaters. This model was chosen because it could operate up to 240 VAC and 50 A.

A program was written in Labview which served as the thermostatic control for each pair of heaters. The temperatures under each pair of heaters were measured with thermocouples and read into the control computer. The temperatures were averaged and that average was used as the control variable for the thermostat program. A PID(Proportional Integral Derivative) algorithm was used as the basis for the thermostatic control. The errors, or deviations of the the control variable from the set point, are accumulated and used by the PID algorithm to gate the output. Proportional refers to the current error, derivative to the past errors, and integral to the predicted future errors. Weighting factors can be applied which can place different levels of importance on each type of error. The output of the PID had a range of 0 - 100% and this value was used to control the duty cycle of the heaters.

For example, if the average of the floor temperature was well below the desired set point, the PID might yield an output of 100%. This meant that for 1 cycle of time, 1 second was used for our controller, the contacts of the solid state relay should be closed the entire 1 second. If the average of the floor temperature was nearing the desired set point the PID may yield an output of 50%. This would cause the contacts of the solid state relay to be open for 0.5 seconds and closed for 0.5 seconds. If the floor temperature exceeded the desired set point the PID would always yield a 0% output and no current would be allowed to pass through the heaters.

The PID controller had to be tuned so as to find the optimum weighting values

for the proportional, integral, and derivative gains. Every system is different but a Ziegler-Nichols tuning scheme can be used to find the optimum weighting values that will provide a satisfactory system response. A Ziegler-Nichols tuning scheme was applied to the heater system for a set point of $150°F$ and a tunnel flow speed of 30 ft/s. When the tuning scheme was completed the lower surface of the wind tunnel could be held constant at $150\pm2°F$.

The heated floor panels worked relatively well as designed but there were some undesirable performance issues. One unanticipated consequence of the heated floor design was the thermal expansion of the tin sheet metal layer. When the floor temperature was raised the sheet metal layer would expand. Since the sheet metal was firmly affixed to the plywood layer beneath it caused the entire panel to warp. The panel actually deflected about 3/8" in the center. The deflection of the panels due to the thermal expansion of the sheet metal layer can be seen in Fig 2.6 and Fig 2.7.

2.4 Traverse System and Pitot-Static Probes

To accurately map out the flow profile in the tunnel test section, a traverse system and a pitot-static probe were used. A pitot-static probe is commonly used to measure low flow speeds because at low flow speeds the fluid still exhibits incompressible behavior, so Bernoulli's equation can be used. Bernoulli's equation is given in Eq 2.2 and is valid for any two points along a streamline where the flow is steady and incompressible.

$$\frac{p_1}{\gamma} + \frac{V_1^2}{2g} + z_1 = \frac{p_2}{\gamma} + \frac{V_2^2}{2g} + z_2 \tag{2.2}$$

In Eq 2.2, p is the absolute pressure, γ is the specific gravity of the fluid, V is the fluid velocity, and g is the gravitational acceleration. A typical pitot-probe is

Figure 2.6. Isometric view of warped heater panel.

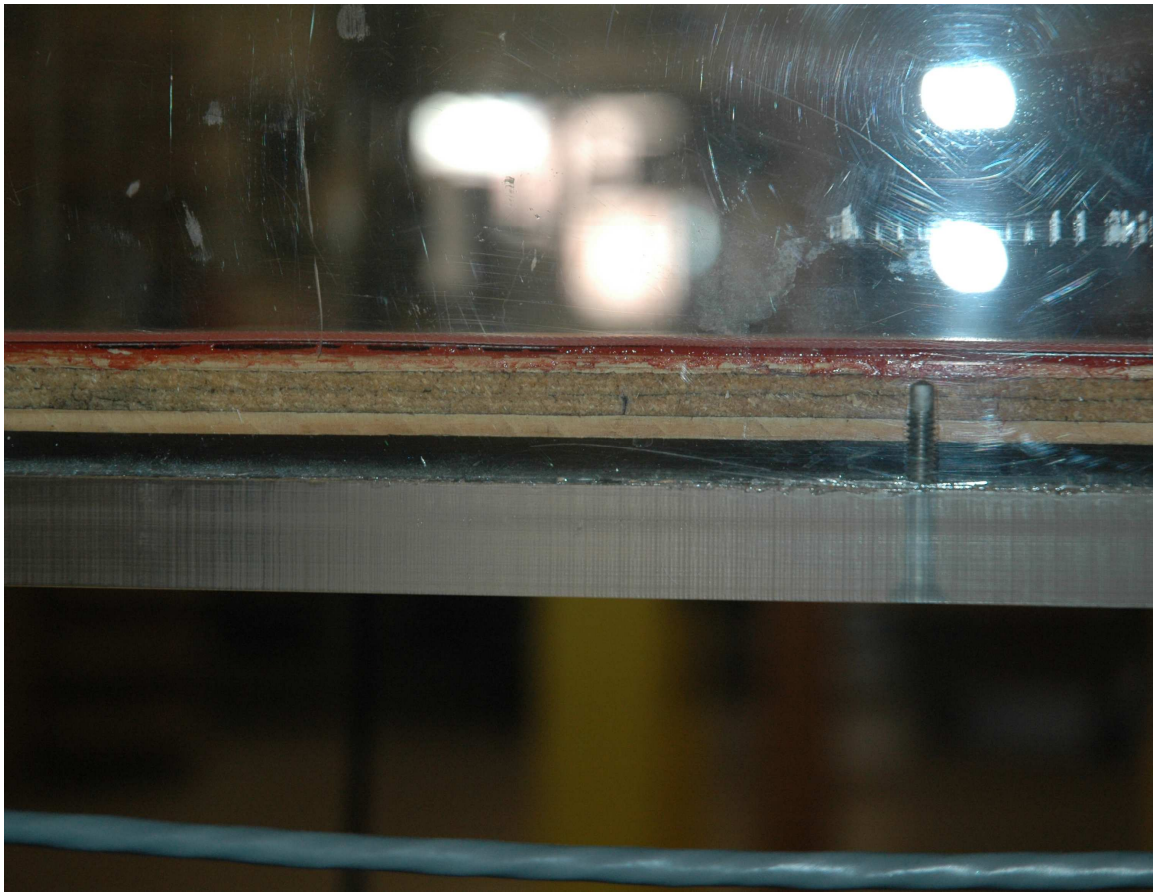

Figure 2.7. Side view of warped heater panel.

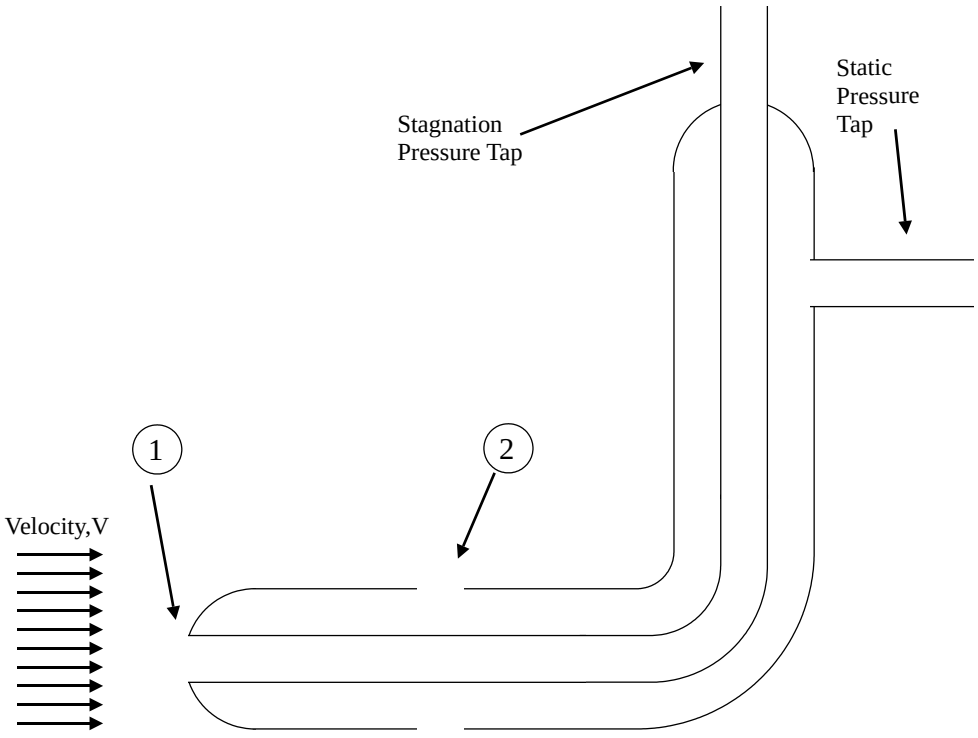

Figure 2.8. Schematic of a standard pitot-static probe.

shown in Fig 2.8. As the fluid flows past the probe the flow stagnates at location 1. Ports 1 and 2 are essentially at the same elevation and on the same streamline so the pressure difference between them can be used to solve for the velocity at location 2.

The fluid's specific gravity γ is also related to the fluid's density and gravity by Eq 2.3.

$$\gamma = \rho g \tag{2.3}$$

Substitution of Eq 2.3 into Eq 2.2 and utilizing the ideal gas law

$$P_{atm} = \rho R T_{atm} \tag{2.4}$$

and solving for V_2 yields the pitot tube equation given in Eq 2.5. Eq 2.5 was the basis for determining the mean velocity profile throughout this experiment. The fluid density could be determined by measuring the atmospheric pressure and temperature of the air entering the wind tunnel. By now knowing density, and using the pitot probe to measure the stagnation and static pressure, the flow velocity in the wind tunnel could be solved for.

$$V_2 = \sqrt{\frac{2(p_1 - p_2)RT_{atm}}{p_{atm}}} \tag{2.5}$$

For this experiment two pitot-static probes were used. One probe was inserted in the side of the wind tunnel midway up the side wall and immediately at the beginning of the test section. This probe was used to find a reference free-stream velocity for the tunnel. Any references made to the tunnel speed are referring to the velocity at this point. The second pitot-static probe was inserted through the top wall of the test section and was attached to a traverse system. The traverse system used was a Velmex Bi-Slide mechanism with a SmartMotor servomotor which allowed for precise automated movement of the pitot-static probe throughout the test section.

A Pressure Systems 9016 Ethernet Pressure Scanner with 10" H_2O, 0.3612 psi, maximum range sensors was connected to the pitot-static probes and used to acquire the pressure data. An Omega K-type thermocouple was connected to a Keithley Temperature scanner to measure the room temperature. A Pressure Systems 9032 Ethernet Barometer was used to measure the barometric pressure in the room. The barometric pressure and room temperature were used to determine the density of the air entering the wind tunnel. A Labview interface was created which would read in the stagnation and static pressures from each pitot-static probe, the barometric pressure, and the ambient room temperature.

A series of desired coordinates for the location of the pitot-static probe would be read by the Labview program. The program would calculate the tunnel's reference velocity and if that velocity was within a certain tolerance of a desired tunnel set point, then the program would log pressure data from the other pitot-static probe. 20 data points were taken at each coordinate location and averaged. Once the 20 data points were collected, the traverse system would move the probe to the next coordinate location.

The uncertainty of the velocity measurement deduced from the pitot-probe was dependent on the uncertainties of all the measured quantities which were used to solve for the velocity. The equation for the uncertainty of the velocity measurement is given below in Eq 2.6 as

$$u_V = \sqrt{(u_{P_s}\frac{\partial V}{\partial P_s})^2 + (u_{P_o}\frac{\partial V}{\partial P_o})^2 + (u_{P_{atm}}\frac{\partial V}{\partial P_{atm}})^2 + (u_{T_{atm}}\frac{\partial V}{\partial T_{atm}})^2} \qquad (2.6)$$

where u_V, u_{P_s}, u_{P_o}, $u_{P_{atm}}$, and $u_{T_{atm}}$ are the uncertainties associated with the velocity, static pressure, stagnation pressure, atmospheric pressure, and atmospheric temperature respectively. The same type of pressure sensor was used to measure the stagnation and static pressures and it had an uncertainty of 0.0005418 psi. The uncertainty of the barometric pressure gauge was 0.0016 psi and the uncertainty of the K-type thermocouple was about $2°F$. Taking the partial derivatives of Eq 2.5 with respect to each variable and solving for the velocity and uncertainty for typical reference tunnel conditions of approximately 30 ft/s, the uncertainty in the velocity measurement was about 1.6 ft/s.

2.5 Dynamic Sensors

It was shown in Section 1.3 that surface pressure fluctuation measurements beneath a turbulent boundary layer can give information about the velocity profile above them. To obtain velocity information from the surface pressure measurements, multiple sensors are needed and temporal-spatial correlations need to be made between them. Because the boundary layer was expected to be several inches thick and its profile logarithmic, sensors were mounted in the new heated floor of the tunnel in a logarithmic spacing with varying distances.

The original sensors used in the experiment were 3/32" diameter 5 psi differential Kulite XCQ-093 series pressure transducers. The sensitivity of these sensors were all nominally 0.020 V/psi. After considerable trial and error and attempts at data acquisition with these sensors it was finally determined that these sensors were not suitable for this experiment. The wiring leading up to the transducers is very small, #36 AWG, and was not shielded. No usable data was ever able to be obtained from these sensors because they were susceptible to picking up extraneous electrical noise. Because the Kulite pressure transducers were surface mounted in the heated bottom floor they were exposed to considerable amounts of electrical noise from the heating pads. The Kulite pressure transducers were replaced with 1/4" Panasonic series WM-61A omnidirectional back electret condenser microphones. These sensors were much more sensitive than the Kulite sensors; the Panasonic sensors had a nominal sensitivity of 150 V/psi as compared to 0.020 V/psi for the Kulite sensors. The increased sensitivity of the Panasonic microphones allowed the very small surface pressure fluctuations to be detected above the electrical noise floor. The Panasonic sensors had a specified frequency range of 20-20,000 Hz where the sensor responded with a uniform sensitivity. Data from this experiment is given for frequencies below

20 Hz and it should be noted that it is uncertain whether the sensor responded below 20 Hz in the same manner as it did above 20 Hz because no manufacturer's specifications were given.

Due to their increased diameter, the Panasonic sensors could not be flush mounted into the heated floor as was previously done with the Kulite sensors. Because the two heating pads butted up directly next to one another, if a hole was enlarged in the heated floor to accomodate the new sensors, the internal wires of the heating pad would inevitably have been cut and the heating pads would not function.

A curved thin strip of wood was cut with a channel routed into the underside of it. The sensors were flush mounted with the top surface of the wooden piece and all the wiring for the sensors could be run inside of the channel and out of the wind tunnel. A cross-sectional view of the wooden piece in which the sensors were mounted is shown in Fig 2.9.

Two of these pieces were cut 48" long, one for each of the flooring sections. 1/4" holes were drilled in the top of the wooden trim pieces for the sensors to be mounted. The sensors were held in place to the wood trim with adhesive applied to the bottom of each sensor and to the wood by way of a hot glue gun. Once all of the sensors had been mounted and all of the sensor wires were run into the channel on the underside of the wood, 3/16" thick high-temperature adhesive fabric tape was attached to the underside of the wood trim to cover the wiring. The idea behind this was to try to insulate the sensor wiring from the heater pads directly beneath them.

The sensors were all connected to Endevco Model 316 DC Differential Voltage Amplifiers. The amplifiers were connected to a National Instruments PXI-4462 24-bit analog to digital converter capable of a 204.8 kHz sample rate. A Labview program was created for data acquistion from the sensors and a range of ± 1 volts was used.

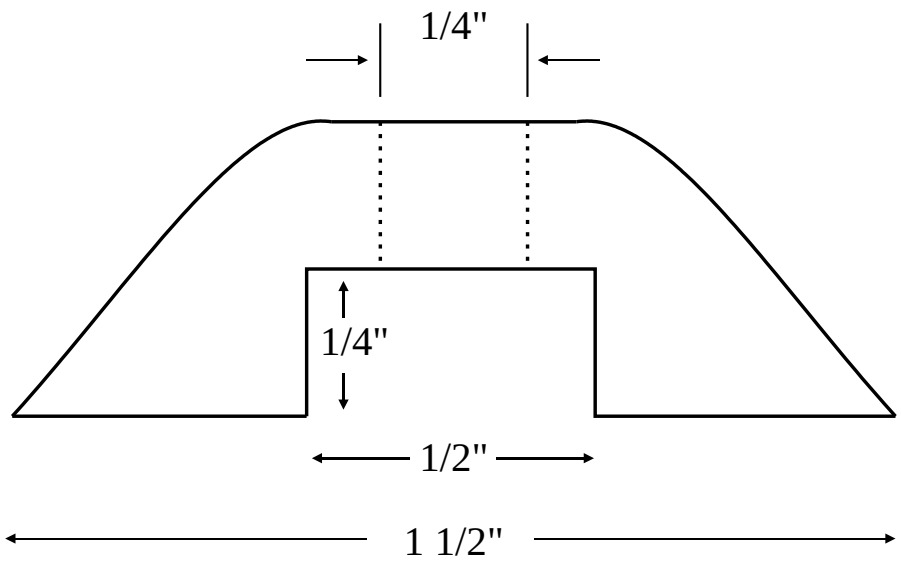

Figure 2.9. Cross-sectional view and dimensions of wooden trim piece used to mount pressure transducers.

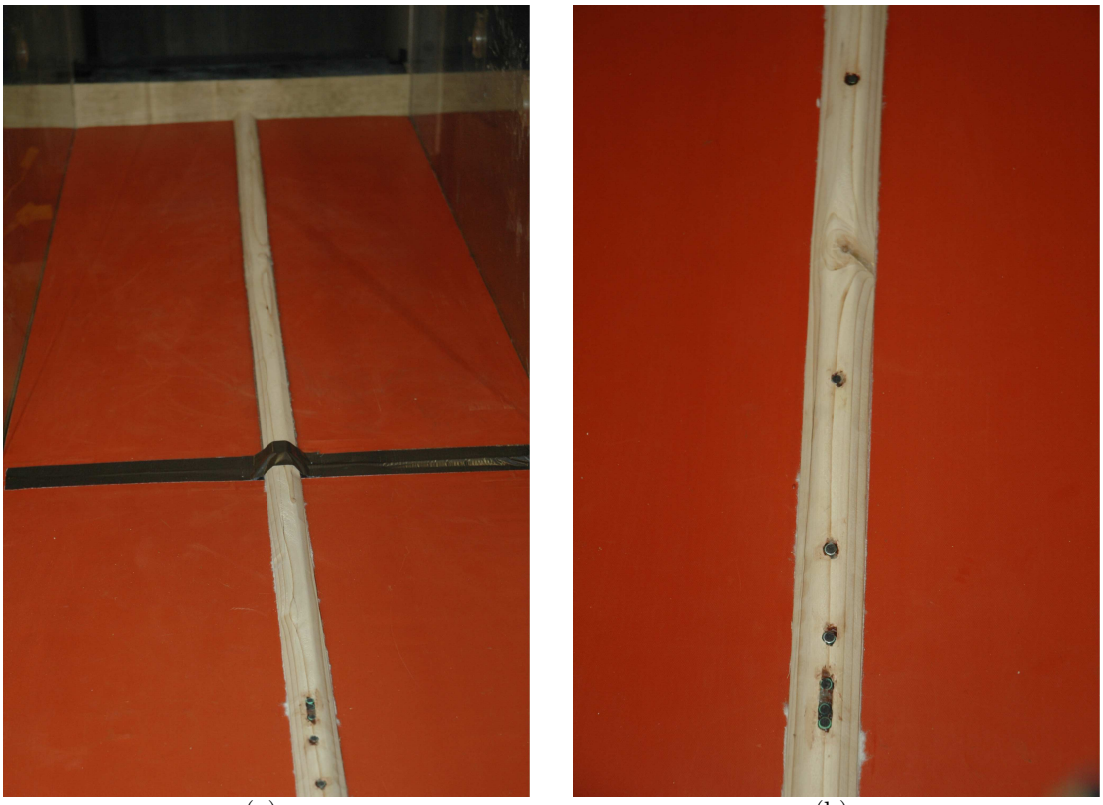

(a) (b)

Figure 2.10. 2.10(a) showing the two wooden trim pieces installed on the bottom floor of the wind tunnel test section and 2.10(b) showing the logarithmic spacing of the surface mounted pressure sensors. The flow direction is from top to bottom.

The A/D converter would automatically oversample data so as to create a digital filter with a cut-off at half of the desired sampling frequency. No analog filter was used in the data acquisition.

A calibration method was needed to determine the sensitivity of each of the sensors. A Brüel & Kjaer Type 4226 Multifunction Acoustic Calibrator was used to excite each individual sensor at a known frequency and sound pressure level. The setup of the calibration system is seen in Fig 2.11. The small cylindrical portion seen in Fig 2.11 contains a 1/4" Brüel & Kjaer microphone which is driven backwards and used as a speaker.

The sensor to be calibrated is usually slid into a coupler where it is sealed on the sides with an o-ring. Because our sensors were flush mounted they could not be placed into the coupler for calibration. This problem was solved by placing an o-ring on the top face of the calibrator coupler. The calibrator was placed on top of the wood trim piece and held down with a steel weight so as to create an airtight seal so that all of the sound produced by the calibrator would be seen by the flush mounted sensor.

The sensitivity of the sensors could be determined by

$$Sens = \left(\frac{V_{rms}}{P_{rms}}\right) \tag{2.7}$$

where V_{rms} is the root mean square voltage detected by the sensor for a constant amplitude, constant frequency, pressure signal. The sound pressure level can be described by

$$SPL = 20\log_{10}\left(\frac{P_{rms}}{P_{ref}}\right) \tag{2.8}$$

where P_{rms} is the root mean square pressure and P_{ref} is some reference pressure,

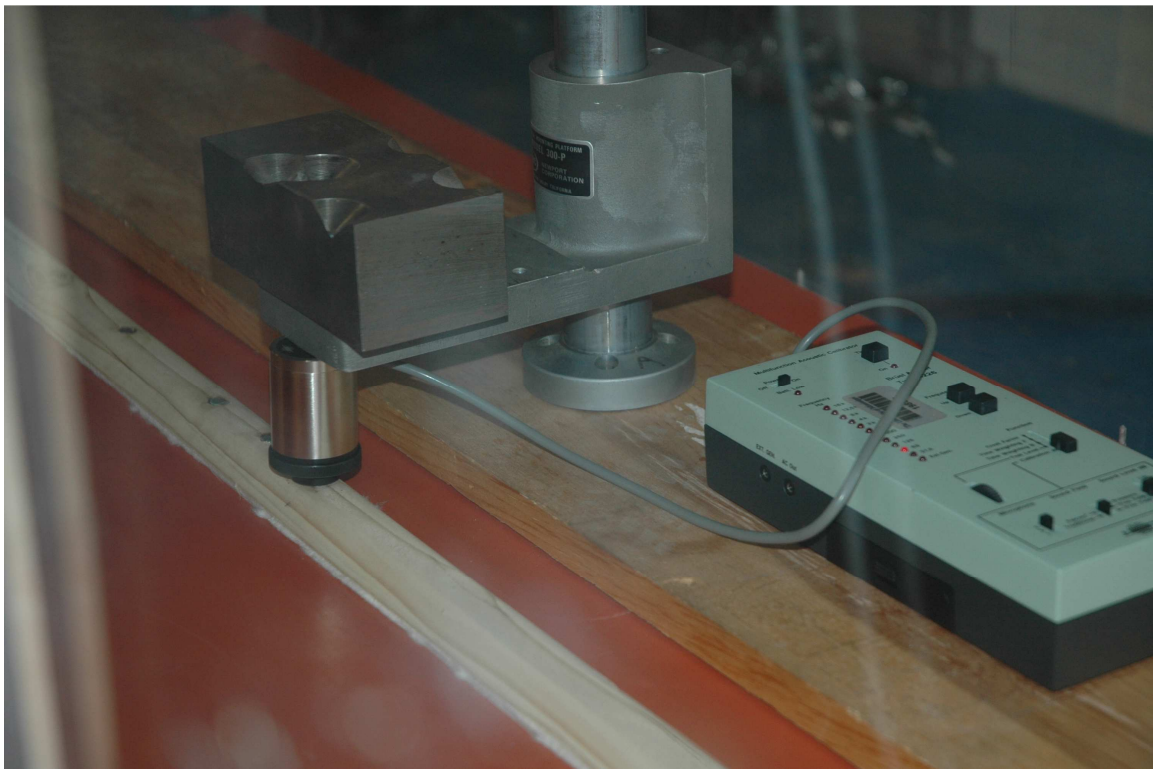

Figure 2.11. Setup of calibration system for pressure transducers.

20 μPa in this case, and SPL is the sound pressure level in decibels dB. The flush mounted sensors were all calibrated for a SPL of 94 dB at 63 Hz. 1,048,576 samples of the sensor's output voltage were taken for each calibration. The root mean square of the voltage signal was divided by the root mean square pressure associated with 94 dB, 1.00237 Pa or 1.45382×10^{-4} psi, to obtain the sensitivity of each sensor. The sensitivities of the sensors were all in the vicinity of 150 V/psi.

Chapter 3

Mean Flow Measurements

3.1 SolidWorks Flow Simulation

Before any modification was done to the wind tunnel, a flow simulation was carried out using SolidWorks to verify that a thick boundary layer could be produced for flow over a backward facing step. A two-dimensional model was created in the program having the exact same dimensions as the wind tunnel test section. Before the simulation could be carried out a grid had to be created to define the flow simulation area. It was known from boundary layer theory that the largest velocity gradient would be near the wall. A very small grid spacing would be required near the walls so as to properly resolve the boundary layer profile. A grid spacing of 1/32" was used from $0 < y < 4$ and $20 < y < 24$ and a grid spacing of 1/8" was used from $4 \leq y \leq 20$. A grid spacing of 1" was used for the entire x-direction because the velocity gradient in the x-direction was not anticipated to be very great. The flow simulation was carried out for an inlet velocity of 30 ft/s and lower wall temperatures of 70°F and 150°F.

The results of the SolidWorks flow simulation for $T_w = 70°\text{F}$ can be seen in Fig 3.1. Dark red corresponds to the highest flow speed and dark blue corresponds

Figure 3.1. X-velocity contour plot of a SolidWorks flow simulation at 30 ft/s.

to the lowest flow speed. It is clearly seen from Fig 3.1 that as the flow moves over the step it separates and reattaches at a point downstream of the step. A vortical recirculation region can be seen immediately behind the step as indicated by the blue color, representing a negative velocity in the downstream direction. After the flow reattaches a developing boundary layer can clearly be seen by the changing of colors. A very thin boundary layer can also be seen growing on the top surface.

It should be noted that for these simulations the velocity profile at the inlet was given as a single constant value. The section of the bottom and top walls immediately upstream of the step were specified to be ideal walls, which in SolidWorks means the no-slip condition does not apply. These simulations were analogous to having constant velocity inflow condition right at the edge of the backward facing step.

Fig 3.2 shows a boundary layer profile at several locations downstream of the step for the results obtained from the SolidWorks flow simulations. The distance downstream of the step and the vertical distance from the bottom wall were both non-dimensionalized by the step height. It is clearly seen that at a downstream location $x/H = 4$ the flow is still detached from the bottom wall and reattaches at some point before $x/H = 8$. Le *et al.* (1997) showed that the flow would reattach at a downstream location of $x/H = 6.28$ but their simulation was carried out for Re_H of 5100 whereas this simulation was run at Re_H of 50,000. Their simulation

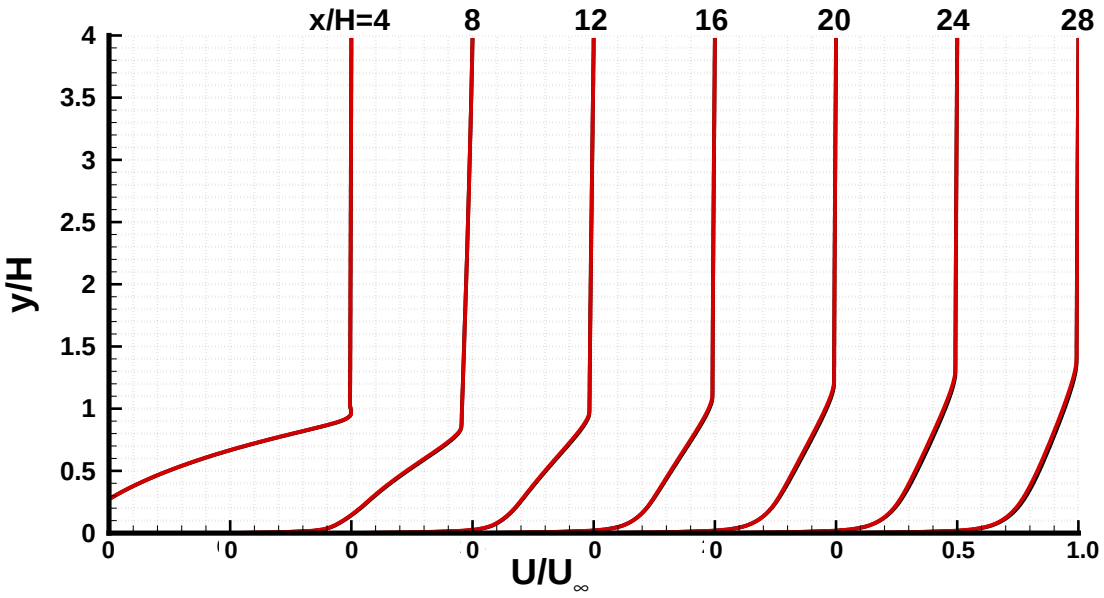

Figure 3.2. Non-dimensional boundary layer profiles at several locations downstream of the step for the SolidWorks simulation at 30 ft/s inlet velocity. Black and red correspond to floor temperatures of 70°F and 150°F respectively.

also differed from this one in that the inlet velocity profile used obeyed the no-slip condition and had a boundary layer thickness of 1.2H at the edge of the step. It is also seen in Fig 3.2 that after the flow reattaches the boundary layer profile exhibits a point of inflection; this point of inflection can be seen out to about $x/H = 16$.

The boundary layer clearly grows with distance downstream of the step to a value of $\delta \approx 1.3H$ at a downstream distance of $x/H = 24$. This corresponds to an actual boundary layer thickness of 3.9" at 6′ downstream of the step. The velocity distribution calculated from this simulation suggested that a sufficiently thick boundary layer could be created downstream of the step in which to take surface pressure fluctuation measurements. The simulations were nearly identical for each surface temperature.

3.2 Pitot-Probe Measurements

A pitot-probe and a traverse system were used to map out the velocity profile in the tunnel test section behind the backward facing step. Data was taken at several locations downstream corresponding roughly to the same shown in Fig 3.2 as well as downstream locations directly over the surface mounted pressure transducers. Data was taken in 1/8" increments from the surface of the bottom wall up to a height of 6" and then 1/4" increments were used for the rest of the data collection. Data was taken for two different floor temperatures, 70°F and 150°F. The non-dimensional velocity profile at several locations downstream of the step can be seen in Fig 3.3. As was shown by Le *et al.* (1997) and the SolidWorks simulation discussed earlier, the flow reattaches somewhere between $x/H = 3.5$ and $x/H = 7.5$ which agrees with the data presented in Fig 3.3. It is not clear the exact point at which the flow reattaches because data was not taken at enough locations in the vicinity of the reattachment to resolve it. This is of no matter because the boundary layer over the surface pressure sensors is of more concern. Just as was shown from the SolidWorks simulation an inflection point exists in the boundary layer profile but the experimental results differ from the simulation in that the inflection point is not seen as far downstream.

The boundary layer profiles differ slightly for the different floor heating conditions for downstream distances of $x/H = 3.5$, $x/H = 7.5$, and $x/H = 11.5$. At further downstream locations the boundary layer profiles for the different floor temperatures are in good agreement. The boundary layer clearly grows downstream after the point of reattachment and reaches a height of $\delta \approx 2H$ at a downstream location of $x/H = 27.5$. By contrast the boundary layer thickness for the SolidWorks simulation was $\delta \approx 1.3H$ at $x/H = 28$. Fig 3.4 shows the non-dimensional boundary layer profile at 63.5" downstream of the step, corresponding to the location of the first

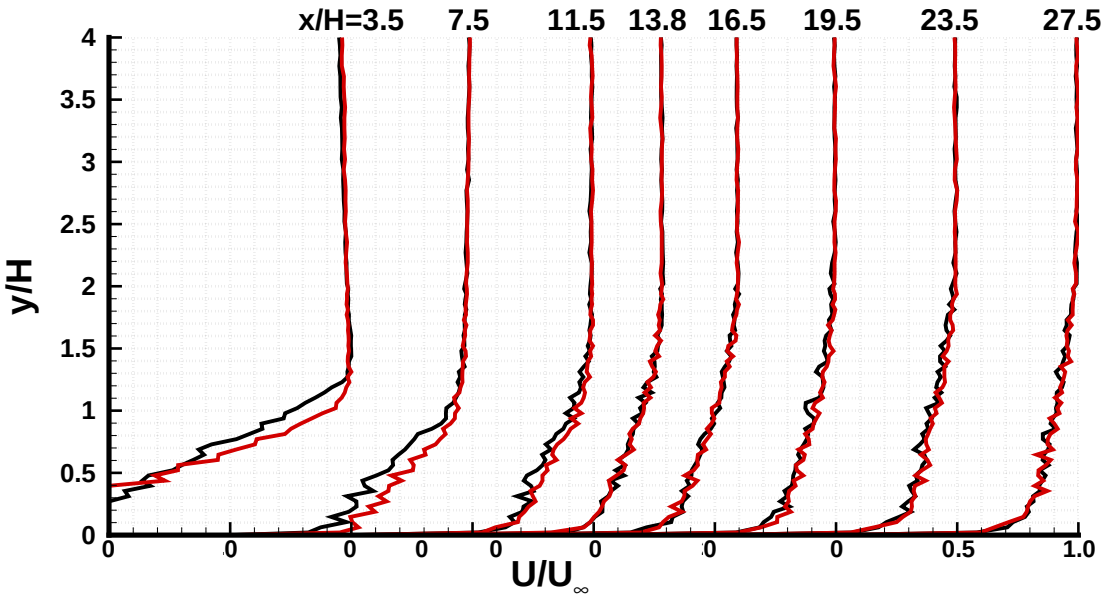

Figure 3.3. Non-dimensional boundary layer profiles at several locations downstream of the step for data taken at a reference inlet velocity of 30 ft/s. Black and red correspond to floor temperatures of 70°F and 150°F respectively.

surface mounted pressure sensor, for a wall temperature of 70°F. A 1/7 power law approximation is also plotted. The experimental data seems to show that the power law approximation is in good agreement for $y/\delta > 0.2$. Barenblatt *et al.* (1997) showed that the power law provides a good approximation for flat plate boundary layer profiles and is very accurate in the outer layer but not as accurate in the viscous sublayer. All of the boundary layer profiles for locations over the remaining pressure sensors show this same general relationship; they are in good agreement in the outer region but differ from the power law close to the wall.

Fig 3.5 is the same as Fig 3.4 except for a wall temperature of 150°F. Again the boundary layer profile is in good agreement with the power law for values of $y/\delta > 0.2$ but differs from the power law closer to the wall. All of the boundary layer profiles for a floor temperature of 150°F for locations corresponding to the pressure sensors showed similar characteristics.

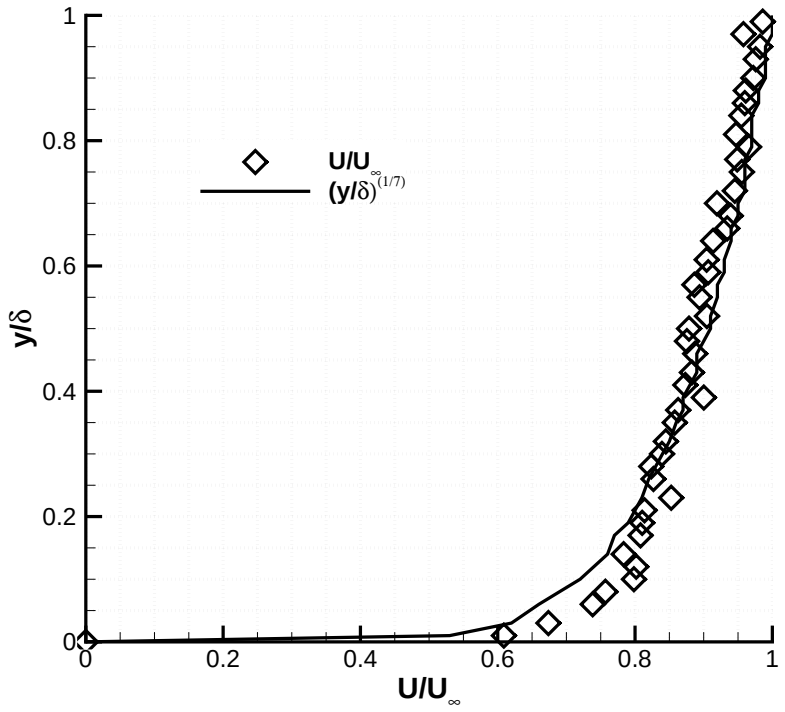

Figure 3.4. Comparison of boundary layer profile with 1/7 power law approximation for downstream location of x=63.5in.,$T_w = 70°$F, and $U_\infty = 30$ft/s.

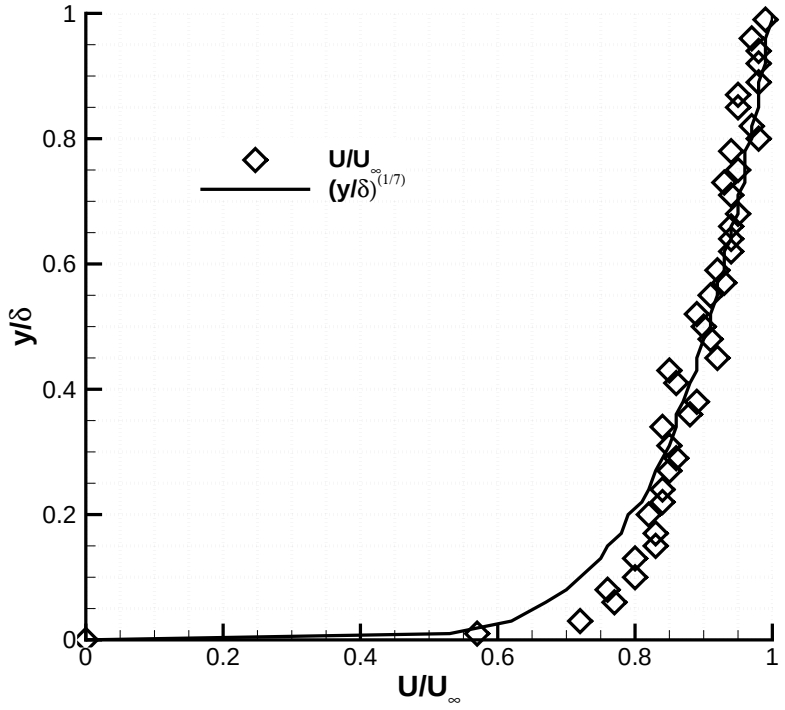

Figure 3.5. Comparison of boundary layer profile with 1/7 power law approximation for downstream location of x=63.5in.,$T_w = 150°$F, and $U_\infty = 30$ft/s.

Fig 3.6 shows the boundary layer data obtained at a downstream location of 90.5" from the backstep compared with a power law approximation and a log-law approximation. An iterative approach was used to fit Eq 1.4 to the experimentally obtained data. Because there was no way to directly measure the shear stress at the wall, the friction velocity, u^*, could not be measured. Values for u^* were incrementally substituted into Eq 1.4 until the experimental data agreed within a prescribed tolerance. At $x = 90.5$ a log-law profile fits the experimentally obtained data within 3% over the entire range of the boundary layer for a friction velocity of 0.904 ft/s. At locations further upstream, where the boundary layer profile still differed slightly from one expected over a flat plate, a log-law profile only agreed with the data within about 6%. This shows that for a Re_H of 50,000, the velocity profile will recover to have the form of a classic flat plate boundary layer after about 30 step heights downstream.

Fig 3.7 shows the non-dimensional boundary layer profiles over the first six surface mounted pressure sensors for a wall temperature of 70°F. It is clearly seen that the boundary layer profiles over the range of the pressure sensors are all self similar and their shape is not changing with increased distance downstream. While the boundary layer does grow ever so slightly over this region, the non-dimensional shape is not changed. Fig 3.8 shows the non-dimensional boundary layer profiles over the first six surface mounted pressure sensors for a wall temperature of 150°F. The profiles all are in clear agreement with one another and demonstrate that the boundary layer profiles are again self similar.

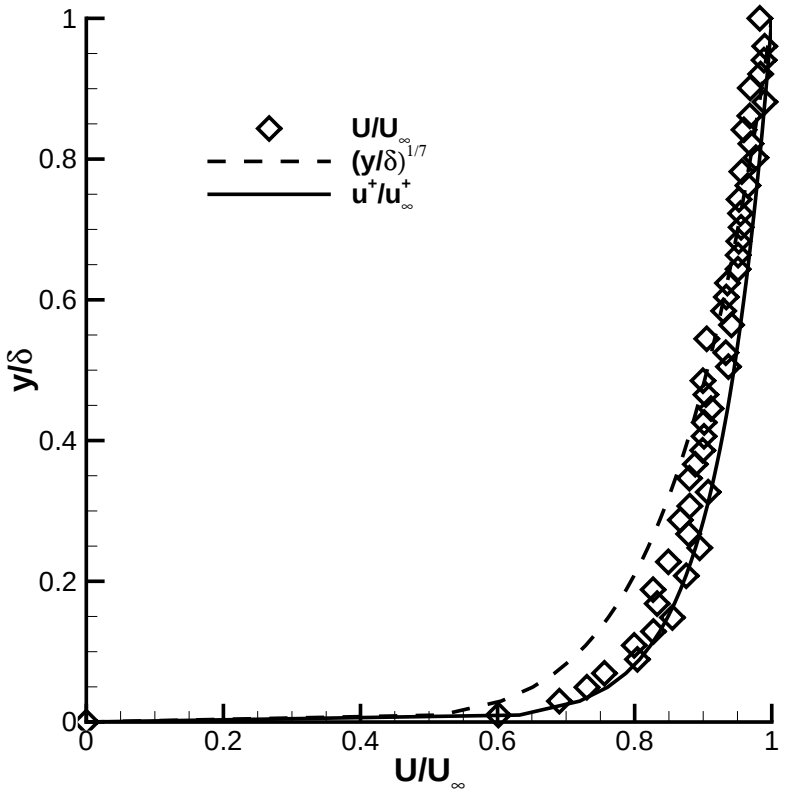

Figure 3.6. Comparison of boundary layer profile with 1/7 power law approximation as well as log-law approximation for downstream location of x=90.5in.,$T_w = 70°$F, and $U_\infty = 30$ft/s.

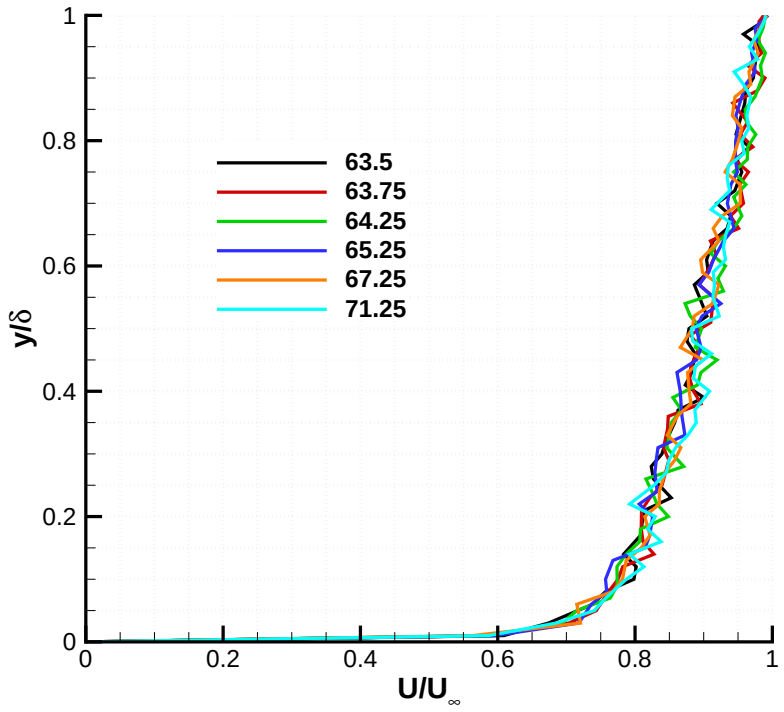

Figure 3.7. Comparison of non-dimensional boundary layer profiles corresponding to locations of surface mounted pressure transducers for $T_w = 70°\mathbf{F}$ and $U_\infty = 30\mathbf{ft/s}$.

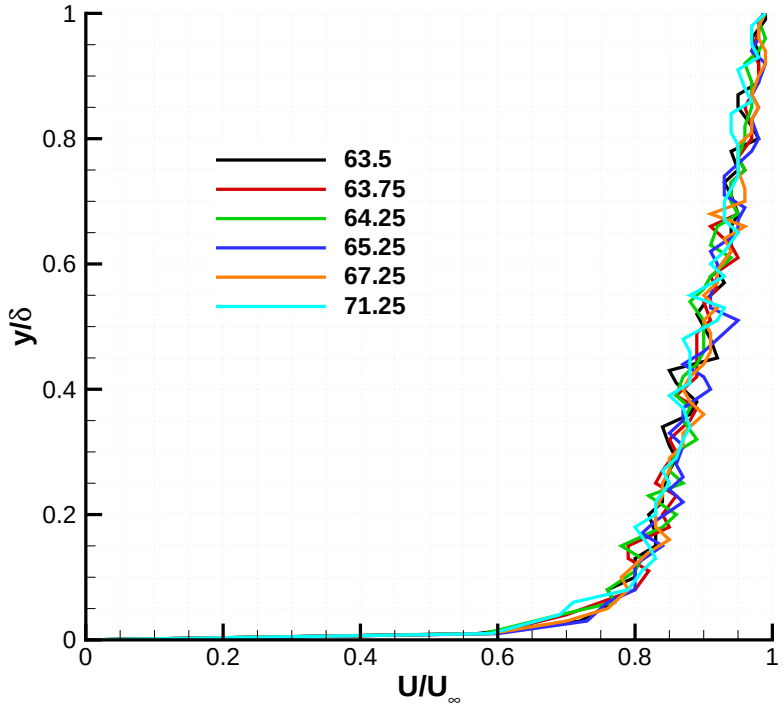

Figure 3.8. Comparison of non-dimensional boundary layer profiles corresponding to locations of surface mounted pressure transducers for $T_w = 150°\mathbf{F}$ and $U_\infty = 30\mathbf{ft/s}$.

Chapter 4

Dynamic Data

4.1 Lighthill's Theory

Lighthill (1952) published a groundbreaking work that described the fundamental theory of aerodynamically generated sound from turbulent flow. Lighthill was trying to create a theory that governed the generation of jet noise but his theory can be applied to all types of aerodynamically generated sound. The theory creates an analogy between an acoustic source in an unbounded medium at rest and a turbulent flow in a quiescent environment. Lighthill's inhomogeneous wave equation is given as

$$\frac{\partial^2 \rho}{\partial t^2} - c_o^2 \nabla^2 \rho = \frac{\partial^2 T_{ij}}{\partial x_i \partial x_j} \tag{4.1}$$

where T_{ij} is Lighthill's stress tensor given below as

$$T_{ij} = \rho u_i u_j + p_{ij} - c_o^2 \rho \delta_{ij} \tag{4.2}$$

where $\rho u_i u_j$ is the Reynold's stress, c_o is the speed of sound in the medium, and p_{ij} is the compressive stress tensor, which for a Stokesian gas can be written by

$$p_{ij} = p\delta_{ij} + \mu \left[-\frac{\partial u_i}{\partial x_j} - \frac{\partial u_j}{\partial x_i} + \frac{2}{3} \left(\frac{\partial u_k}{\partial x_k} \right) \delta_{ij} \right] \tag{4.3}$$

with μ representing the fluid's viscosity. In the case of incompressible, low Mach number flow, Lighthill's stess tensor can be approximated simply as the Reynold's stress and rearranging Eq 4.1 for pressure instead of density yields

$$\nabla^2 p = -\frac{\partial^2 \rho u_i u_j}{\partial x_i \partial x_j} \tag{4.4}$$

An integral solution of Eq 4.4 implies that the pressure is determined, at least nominally, by contributions from all parts of the velocity field (Bull, 1996). Consider the representative, but somewhat idealized, case of the fluctuating wall-pressure field associated with low Mach number turbulent boundary layer flow over a rigid flat surface. For such an idealized case, the boundary layer thickness increases slowly in the direction of the flow and the turbulence in it can be thought of as homogeneous for planes that are parallel to the rigid flat surface. Following this logic, the pressure field at the surface can be represented as a homogeneous spatial field that is stationary in time.

4.2 Data Acquisition and Processing

Since the pressure at any location on the flat surface beneath a turbulent boundary layer has been determined to be a stationary random variable, classical statistical analysis can be applied to pressures measured at multiple locations on the wall to obtain information about the flow. The spatial-temporal cross-correlation function of any two pressure signals measured beneath the turbulent boundary layer can be found by taking the inverse Fourier transform of the cross-spectral density function S_{xy} as shown in Eq 4.7. The cross-spectral density function is shown below as

$$S_{xy}(f) = X^*(f)Y(f) \tag{4.5}$$

where $X^*(f)$ is the complex conjugate of the Fourier transform of the pressure signal at the first location and $Y(f)$ denotes the Fourier transform of the pressure signal at the second location. The Fourier transform of the time dependent pressure signal at any location is given is Eq 4.6.

$$X(f) = \int_{-\infty}^{\infty} x(t) e^{-2\pi f t} dt \tag{4.6}$$

where $x(t)$ is the time dependent fluctuating pressure.

$$R_{xy}(\tau) = \int_{-\infty}^{\infty} S_{xy}(f) e^{j2\pi f \tau} df \tag{4.7}$$

Because the pressure signals were only fluctuations about a zero mean, the value of the cross-correlation function of any pressure signal with itself at $\tau = 0$ yielded the variance of the signal such that $R_{xx}(0) = \sigma_x^2$. By knowing the variance of the pressure signal at any location, a normalized cross-correlation function, or correlation coefficient function, could be calculated by

$$\rho_{xy}(\tau) = \frac{R_{xy}(\tau)}{\sigma_x \sigma_y} \tag{4.8}$$

For free stream flow speeds U_∞ of 15, 20, 25, and 30 ft/s and floor temperatures T_w of 70, 100, 125, and 150°F, the surface pressure fluctuations were measured beneath the turbulent boundary layer which developed on the bottom surface of the wind tunnel test section behind the backward facing step. The pressure sensors were located at downstream locations of x = 63.5, 63.75, 64.25, 65.25, 67.25, 71.25, 79.25, and 95.25" respectively. Once the tunnel had reached steady operating conditions, pressure data was acquired from the sensors at a sampling rate of 4000 Hz. 1,048,576

samples from each sensor were acquired and the resulting data was divided into 128 blocks of 8192 points each. A Fast Fourier Transform (FFT) algorithm, like that shown in Press *et al.* (1992), was used to calculate the Fourier transforms of each block of data of the individual pressure signals. The FFT's of all 128 blocks of data were averaged for each pressure sensor. Having obtained the Fourier transforms of each individual pressure signal, the auto-spectral and cross-spectral density functions could be calculated from Eq 4.5. Applying the same FFT algorithm, the inverse Fourier transforms of the cross-spectral density functions were used to find the spatial-temporal cross-correlation functions between any two sensors. The non-dimensional correlation-coefficient functions were then calculated as shown in Eq 4.8.

The auto-spectral density functions for the pressure signals obtained at each sensor location are seen in Fig 4.1 for all four free-stream flow speeds and a wall temperature of 70°F. The fluctuating pressure for each frequency band is given as sound pressure level in dB relative to a reference pressure of 20 μPa. It is not surprising to see that the values of the sound pressure level increase with increasing flow speed. This is the result of a larger boundary layer where turbulence exists, and thus a larger effect on the values of the surface pressure fluctuations. There are several pronounced spikes seen in all of the spectra of Fig 4.1. It was determined that these spikes are all the result of sound produced from the wind tunnel motor and fan being propagated upstream into the wind tunnel test section. A laser tachometer was used to measure the rotational speed of the fan for each desired tunnel flow speed. The rotational speeds were found to be 288, 357, 443, and 537 rpm respectively for tunnel free stream flow speeds of 15, 20, 25, and 30 ft/s. These rotational speeds correspond directly to frequencies of 4.8, 5.95, 7.38, and 8.95 Hz respectively. All of the spikes seen in Fig 4.1 correspond to these frequencies or their higher harmonics.

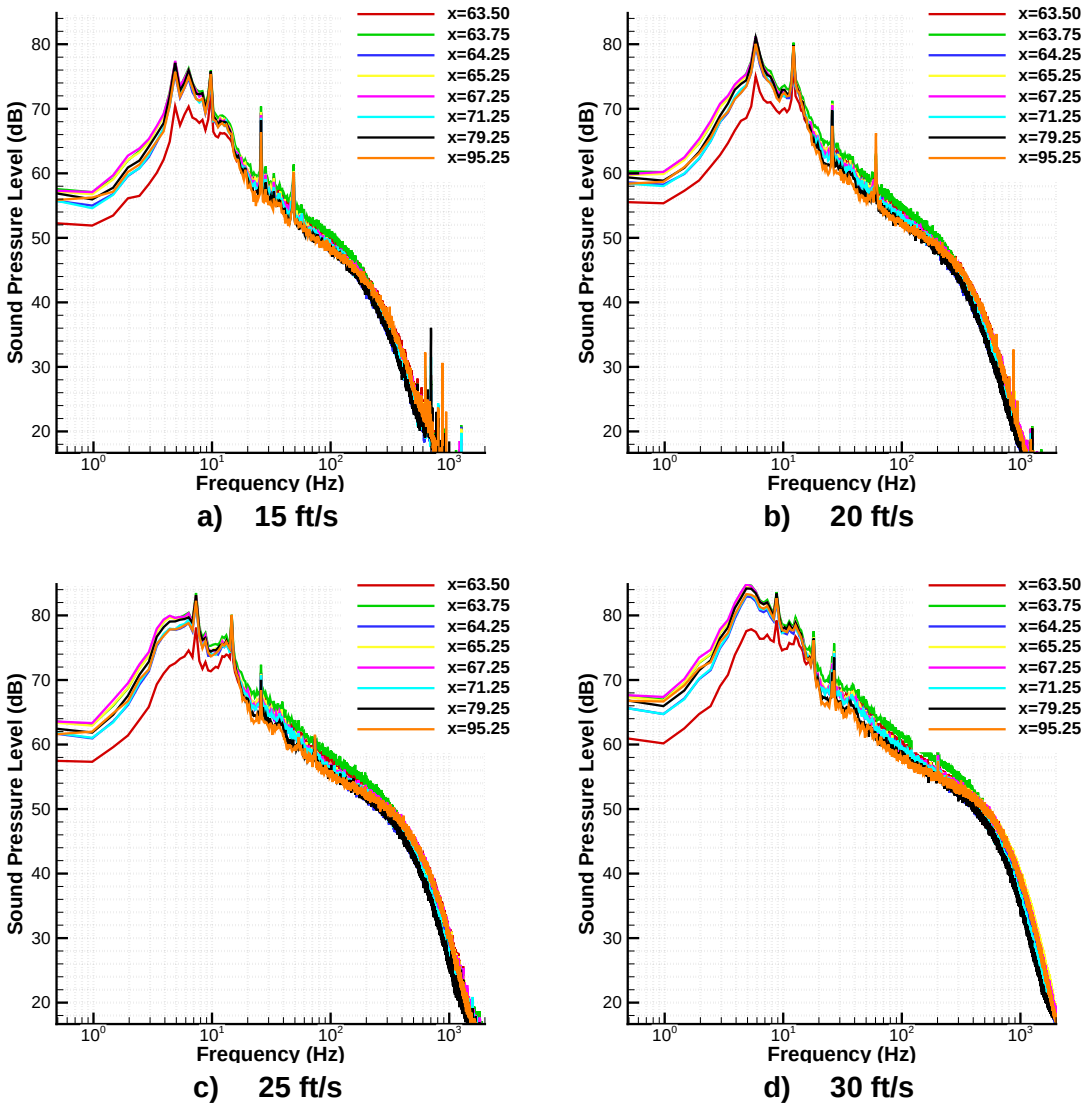

Figure 4.1. Surface sound pressure levels for flow speeds of a) 15 ft/s, b) 20 ft/s, c) 25 ft/s, and d) 30 ft/s for a floor temperature of $70°F$.

The spectra seen in Fig 4.2, which are for a floor temperature of 150°F, appear to be identical to those seen for lower floor temperatures. The main difference that stands out is that a clear 60 Hz peak can be seen for all of the spectra. This peak is the result of the extraneous 60 Hz electrical noise which was produced by the electric heater pads. For low flow speeds, such as seen in Fig 4.2, the electrical noise is almost 20 dB higher than the pressure signal for nearby frequencies, which is quite significant. For all of the data collected, the sound pressure levels obtained from the first pressure sensor mounted at $x = 63.5$" were consistently lower than for the rest of the sensors. It is not clear why this location was so much quieter than the others; the sensitivity of every sensor was calibrated prior to all tunnel runs. It seems highly unlikely that the physical location of the first sensor would actually be quieter than the second sensor which was only located 0.25" away.

It appears that for all flow speeds and all floor temperatures used in this experiment, the bulk of the energy associated with the surface pressure fluctuations falls within the frequency range of 5 - 20 Hz. Bradshaw (1967) and Panton & Linebarger (1974) showed that the largest value of the pressure spectra would occur for a non-dimensional frequency of $\omega\delta/u^* \approx 50$. For the boundary layer calculated at $x = 90.5$" and a free stream flow speed of 30 ft/s, a boundary layer thickness of 6.3126 in" was measured and a friction velocity u^* of 0.904 ft/s was estimated. Using these values and solving for the non-dimensional value $\omega\delta/u^* \approx 50$, the maximum of the pressure spectra could be expected at about 14 Hz. This agrees very well with the data shown in Fig 4.1 and Fig 4.2 for flow speeds of 30 ft/s.

Farabee & Casarella (1991) created an empirical formula to estimate the rms fluctuating pressure beneath a turbulent boundary layer. Klewicki *et al.* (2008) modified their equation to fit their data which was taken for higher Reynolds number. The

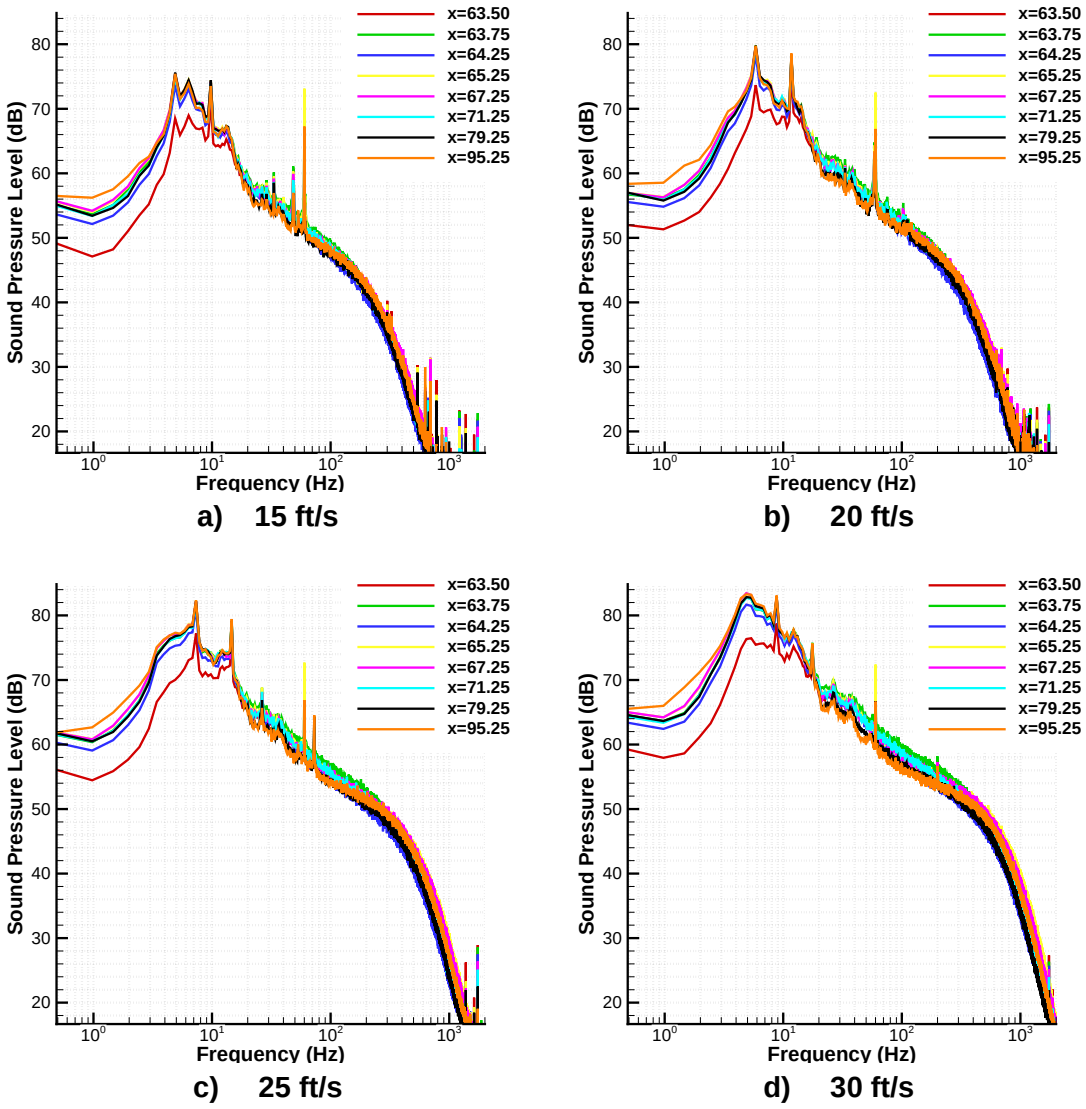

Figure 4.2. Surface sound pressure levels for flow speeds of a) 15 ft/s, b) 20 ft/s, c) 25 ft/s, and d) 30 ft/s for a floor temperature of $150°F$.

estimate for the rms fluctuating pressure beneath a turbulent boundary layer is given as

$$p_{rms} = \tau_w \sqrt{6.5 + 2.30 \ln\left(\frac{\delta^+}{333}\right)} \tag{4.9}$$

where $\delta^+ = \delta u^*/\nu$. Using the values obtained for the boundary layer at $x = 90.5$" and a free stream flow speed of 30 ft/s, the estimated rms pressure over the entire frequency range would be 0.308494 Pa or about 84 dB. The measured overall sound pressure level over the entire frequency range was about 95 dB. The measured values were significantly higher than what would be predicted. After it was found that the Kulite pressure sensors were not sufficiently sensitive for this experiment and the Panasonic sensors were used, the boundary layer over these sensors was never measured. It was hoped that the thin wooden strip holding the sensors would not alter the flow field very much from when the boundary layer profile measurements were made. It could be that the boundary layer over the newly installed sensors was different enough, i.e. the shear stress at the wall and boundary layer thickness were altered, to account for the difference in the overall sound pressure level. Another likely reason for the difference in the expected overall sound pressure level is extraneous noise pollution. It has already been shown that tones from the wind tunnel fan can be clearly observed upstream by the sensors. Farabee & Casarella used acoustic mufflers both upstream and downstream of the test section to minimize extraneous facility noise. It could also be that the pressure sensors were not vibrationally isolated from the wind tunnel and much of the noise which is seen is simply the pressure sensors physically vibrating. Researchers early on realized the need to vibrationally isolate the pressure sensors from the wind tunnel (Willmarth, 1956).

The auto-correlation of each pressure signal was calculated and is shown in Fig 4.3

for a free stream flow speed of 30 ft/s and a surface temperature of 70°F. The highest correlation coefficient comes at $\tau = 0$ for all of the signals as expected. The auto-correlation functions clearly display a periodic decay in time. The period of this decay is approximately 112 ms which corresponds to a frequency of about 8.92 Hz. This is almost the exact frequency spike which was observed in the auto-spectral density functions and was noted to have been caused by extraneous fan noise. All of the curves seen in Fig 4.3 seem to be nearly identical with the exception of the first one. This is no surprise however because the energy of the spectra for the first pressure sensor was much less than the others. The same basic characteristics were observed in all the auto-correlation coefficient functions for all the flow speeds and all surface temperatures. The only differences were the periods of the harmonic decay; fan noise was at different frequencies for different flow speeds. In the case of floor heating, very faint peaks over the larger amplitude ones could be observed. The locations of these very faint peaks corresponded to the 60 Hz electrical noise.

The cross-correlation coefficient functions of every pressure sensor with the first sensor for tunnel conditions of $U_\infty = 30$ ft/s and $T_w = 70$°F can be seen in Fig 4.4. The peaks of ρ_{12}, ρ_{13}, ρ_{14}, ρ_{15} are clearly seen to shift toward increasingly high lag times. By noting the spacing between the sensors in question and measuring the lag time of the highest observed peak, an estimate for the convective turbulent velocity can be made. The shape of ρ_{15} is odd and it appears as though it is bent toward the right. A very faint hump can also be seen at approximately 30 ms for ρ_{16}. This hump could correspond to the turbulent convection lag time. The largest peaks of ρ_{17} and ρ_{18} are not shifted and the curves appear to be very similar to the auto-correlation coefficient functions with the only major difference being their amplitude is only about 0.6. Farabee & Casarella (1991) showed that shifted peaks in the cross-

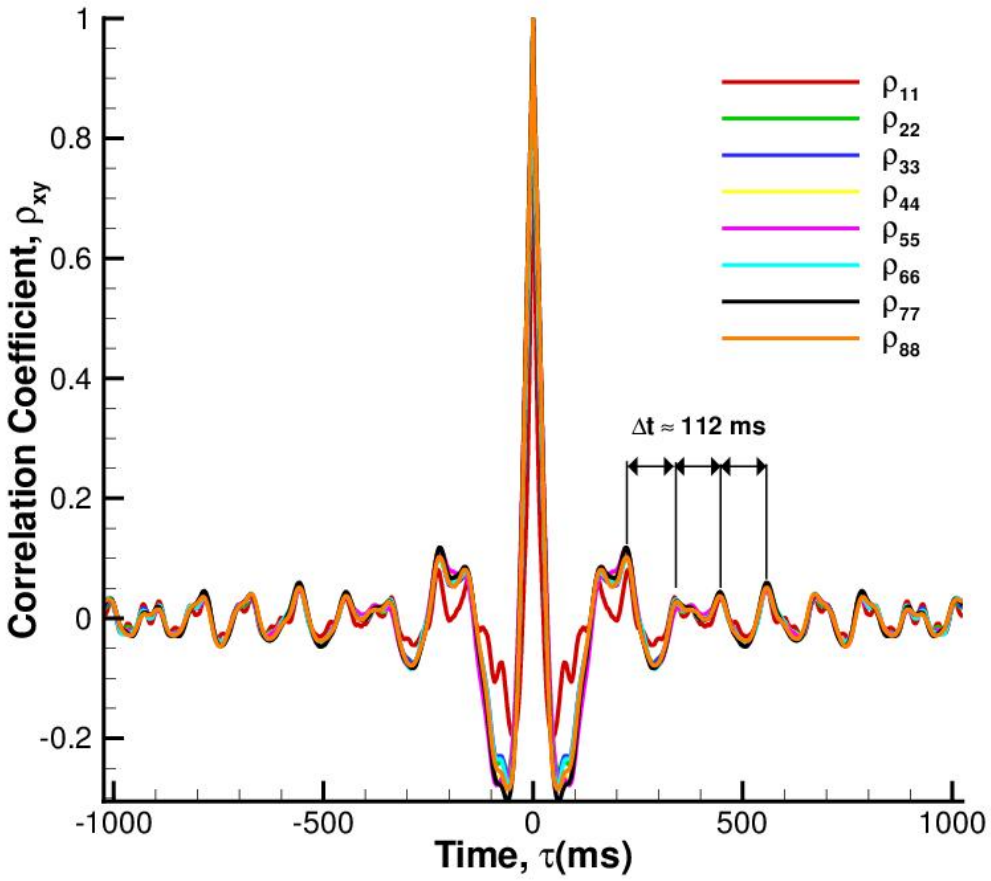

Figure 4.3. Auto-correlation coefficient function of pressure signals obtained for a $U_\infty = 30$ ft/s and $T_w = 70°$F. A periodic decay corresponding to the same frequency associated with the fan noise can clearly be seen.

correlations could be observed for sensor spacings of at least $x/\delta = 6$. The spacings corresponding to ρ_{17} and ρ_{18} are only $x/\delta \approx 2.6$ and $x/\delta \approx 5.3$ respectively so it seems odd that their highest observed peaks would not be seen at some positive lag time. It is believed that the extraneous facility noise and the vibrations of the wind tunnel are causing the signals of each of the pressure sensors to be so strongly correlated with one another at $\tau = 0$. This strong cross-correlation makes it difficult to resolve the peaks corresponding to the turbulent convection.

The cross-correlation coefficient functions for each sensor with all of the other sensors was calculated. This allowed for the maximum number of distance combinations so a finer resolution of the turbulent convection could be had in the downstream direction. Fig 4.5 shows the cross-correlation coefficient functions for several sensor combinations. It is clearly shown that with increasing sensor spacing the lag time of the highest observed peak is also increasing.

It would seem likely that the highest values for correlation coefficient would be for sensors that were spaced closer together. The peak of ρ_{12} is lower than the observed peak of ρ_{23} even though sensor 1 and 2 were spaced closer together. This is due to the fact that the overall sound pressure levels were much closer for sensor 2 and 3 than for sensor 1 and 2. The convective turbulent speed U_c was calculated by dividing the sensors spacing by the time lag associated with the highest observed peak in the cross-correlation coefficient functions.

Table 4.1 shows the calculated convection speeds for $U_\infty = 30$ ft/s for multiple sensor spacings and multiple floor heating conditions. It is obvious that the floor heating has no effect on the turbulent convection speeds observed. For all of the spacings where sensor 1 is involved, the convection speed clearly increases with increased sensor spacing. The convection speed observed for a spacing of 0.5" was

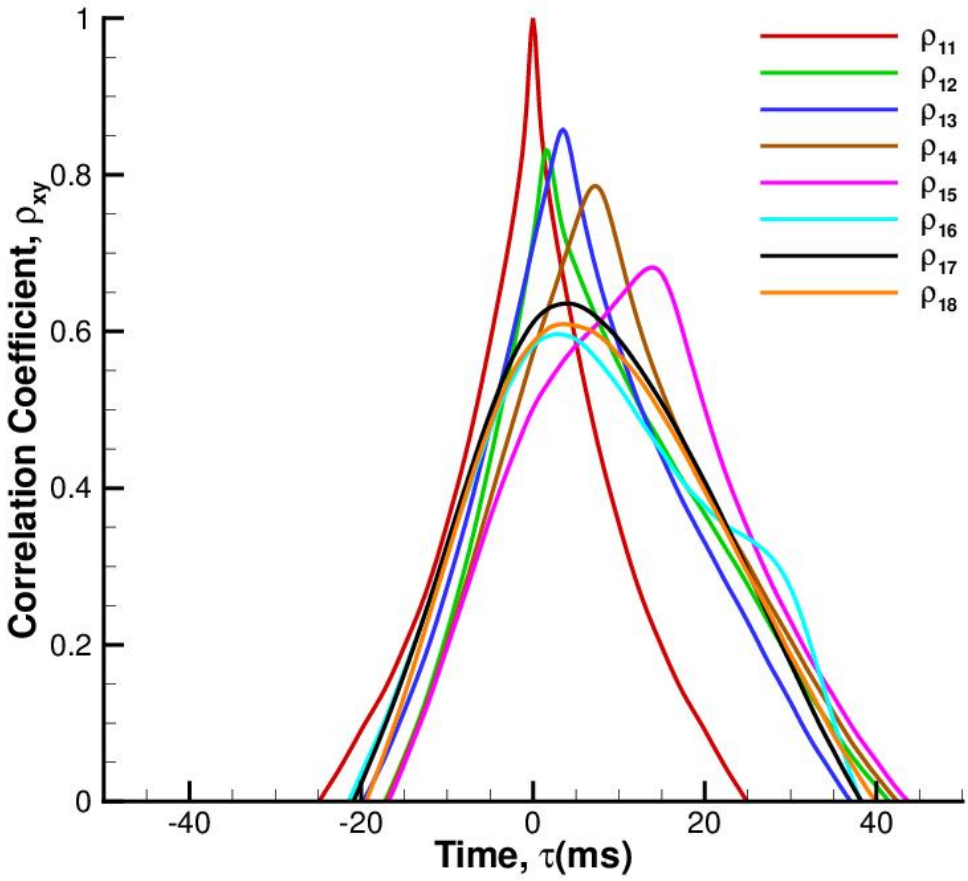

Figure 4.4. Cross-correlation coefficient function of pressure signals obtained for a $U_\infty = 30$ ft/s and $T_w = 70°$F. For larger sensor spacings the maximum observed peak does not shift as expected.

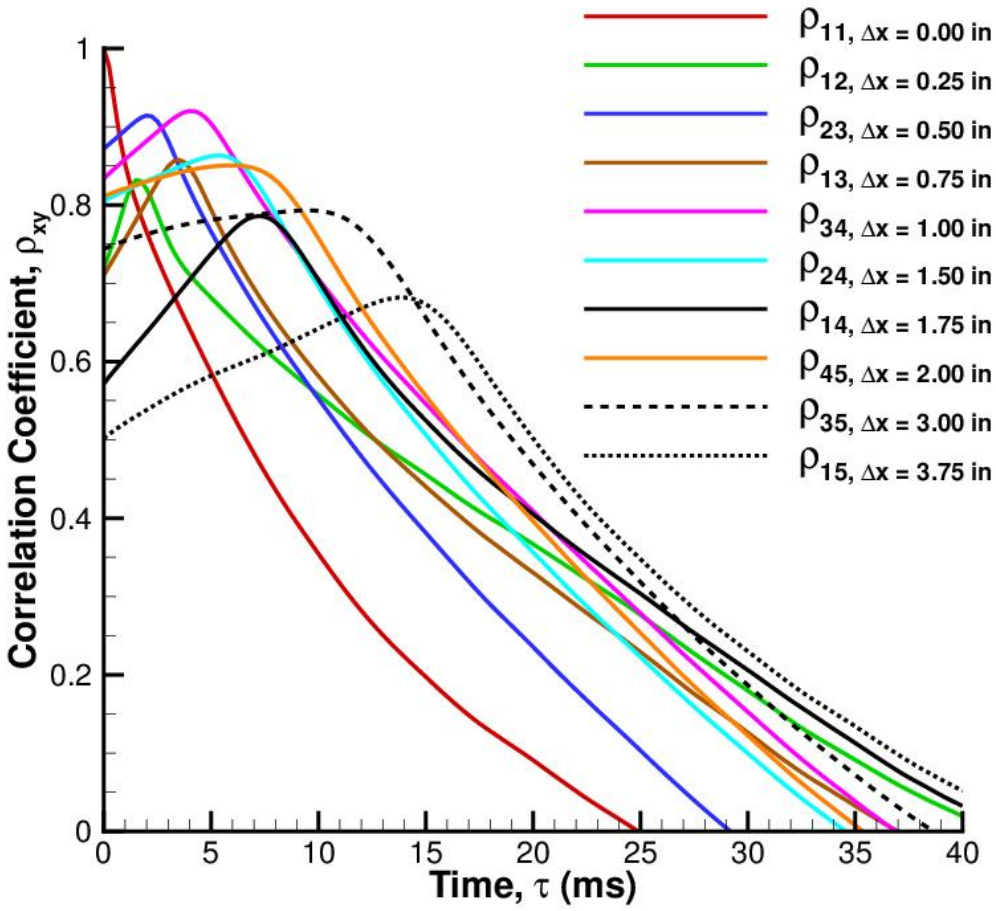

Figure 4.5. Cross-correlation coefficient function of pressure signals obtained for a $U_\infty = 30$ ft/s and $T_w = 70°$F.

		70°F	100°F	125°F	150°F
Δx	ρ_{xy}	Convective Speed, U_c/U_∞			
0.25	ρ_{12}	0.46	0.46	0.46	0.46
0.50	ρ_{23}	0.69	0.69	0.69	0.69
0.75	ρ_{13}	0.60	0.60	0.60	0.60
1.00	ρ_{34}	0.69	0.65	0.69	0.69
1.50	ρ_{24}	0.79	0.79	0.79	0.76
1.75	ρ_{14}	0.67	0.67	0.67	0.67
2.00	ρ_{45}	0.93	0.93	0.97	0.97
3.00	ρ_{35}	0.88	0.83	0.88	0.88
3.75	ρ_{15}	0.76	0.74	0.74	0.74

Table 4.1. Convective speed as a percentage of the free stream velocity calculated for multiple sensor spacings and floor temperatures. $U_\infty = 30$ **ft/s for all cases shown.**

observed to be 69% of the free stream speed but for a spacing of 0.75" the convection speed was only 60%. It is believed that this can be attributed again to the fact that the energy contained in the spectra for the first sensor was nominally lower than for the remaining sensors.

Chapter 5

Conclusions

A current interest exists to use a ground based pressure transducer system to measure the inflow conditions in and around wind farms. This can serve as an input to the control system of wind turbines so they achieve optimum performance while decreasing the damage done to them. For this to be successful a much broader understanding of the problem must be gained. The goal of this experiment was to simply study one component of the broader problem associated with using surface pressure fluctuation measurement to predict flow characteristics. The effect of surface heating on the surface pressure fluctuations and their correlations with flow velocity were studied in a wind tunnel tunnel so as to gain some insight into the phenomena that may exist in the full scale atmospheric boundary layer.

A backward facing step was installed at the front of the wind tunnel test section which served to create a thick, $\delta \approx 6$", boundary layer further down the test section where surface pressure fluctuation measurements were made. A simulation of the flow field was created using SolidWorks. The results of the simulation showed some of the same characteristics that were measured during the actual experiment but the boundary layer thickness as determined from the simulation was much lower than was actually measured.

The boundary layer over the location of the surface mounted pressure sensors was found to be self similar over the entire region and agreed reasonably well with a 1/7 power law approximation for values of $y/\delta > 0.2$. The surface heating did not appear to affect the boundary layer and nearly identical profiles were measured for floor temperatures of 70°F and 150°F. The boundary layer also seemed to agree very wall with that of a classic flat plate boundary layer at a downstream distance of $x/H = 32$.

The sound pressure levels measured beneath the turbulent boundary layer were found to be dependent on the flow speed but the surface heating had little to no effect. The sound pressure levels measured for the first sensor were consistently lower than the others; the cause of this was never determined. The acoustic properties of the wind tunnel which was used were not very good. Acoustic tones could be detected in all of the spectra which were directly related to the frequency at which the fan was rotating. The measured sound pressure levels were found to be about 11 dB higher than would be expected for a flow of this type. It was surmised that this is the result of facility noise and the sensors not being vibrationally isolated from the wind tunnel.

The cross-correlation coefficient functions between multiple sensors were used to estimate the turbulent convective velocity in the boundary layer. The surface heating was shown to have little to no effect on the values that were calculated. It was difficult to ascertain the peaks associated with the turbulent convection because the sensors were still very strongly correlated with one another for small time shifts. Because of the strong cross-correlation to one another around $\tau = 0$ many of the peaks that would have been able to be observed otherwise were washed out. It is believed that had the pressure transducers been vibrationally isolated from the rest of the wind

tunnel the peaks associated with the turbulent convection would have been much more pronounced and easier to obtain.

Chapter 6

Future Work

As with most research, the results usually provide more questions than answers. After the new pressure sensors were installed the boundary layer was never measured over them. New boundary layer measurements need to be carried out for this new modification. The results of this may be able to explain the difference in the measured sound pressure level and that which was expected. The wind tunnel should also be modified so as to eliminate any of the other extraneous facility noise that can be seen in the test section. This may be accomplished by lining the walls of the diffuser with some sort of sound absorbing material. Some effort needs to be made so as to vibrationally isolate the pressure sensors from the vibrations of the wind tunnel test section.

No measurements were made in the present study of the turbulence of the boundary layer. Hot wire anemometry will be used to hopefully obtain information about the correlations of the surface pressure fluctuation to the turbulence at various points in the boundary layer. This will be conducted for various floor heating condtions so as to shed more light on the problem when surface heating is involved. By using hot wire anemometry instead of a pitot-static probe to measure the velocity profile, much finer resolution of the boundary layer can be obtained near the wall. Particle

Image Velocimetry may also be a viable option for measuring the velocity profile simulaneously with the surface pressure fluctuations.

The results of this experiment seem to indicate that the surface heating has little to no effect on the surface pressure fluctuation measurements beneath the boundary layer. It was never confirmed however if any buoyant natural convection was ever actually created from the surface heating. Hot wire anemometry will be able to determine if any discernible vertical velocity was created as a result of the surface heating.

It has been shown that statistical analysis of the surface pressure fluctuations beneath a turbulent boundary layer can give information about the flow field above it. More work needs to be done to show that the surface heating of this experiment actually created buoyant natural convection. Once it is confirmed whether or not buoyant natural convection was actually created, then and only then will it be possible to determine whether it has an effect on the surface pressure fluctuations.

Bibliography

Bibliography

Adams, E. & Johnston, J. (1985) "Experimental Studies of High Reynolds Number Backward-Facing Step Flow." In *Proceedings of the Fifth International Symposium Turbulent Shear Flows*, pages 5.1–5.6.

Armaly, B.; Durst, F.; Pereira, J. F.; & Schonung, B. (1983) "Experimental and Theoretical Investigation of Backward-facing Step." *Journal of Fluid Mechanics*, Vol. 127, pp. 473–496.

Barenblatt, G.; Chorin, A.; & Prostokishin, V. (1997) "Scaling Laws for Fully Developed Turbulent Flow in Pipes." *Applied Mechanics Reviews*, Vol. 50, pp. 413.

Blasius, H. (1908) "Grenzschichten in Flu ossikeiten mit kleiner Reibung." Z. Angew. Math. Phys., vol. 56, pp 1-37 English Translation in NACA Technical Memo 1256.

Bradshaw, P. (1967) ""Inactive" Motion and Pressure Fluctuations in Turbulent Boundary Layers." *Journal of Fluid Mechanics*, Vol. 30, pp. 241–258.

Bull, M. (1967) "Wall Pressure Fluctuations Associated with Subsonic Turbulent Boundary Layer Flow." *Journal of Fluid Mechanics*, Vol. 28, pp. 719–754.

Bull, M. (1996) "Wall Pressure Fluctuations Beneath Turbulent Boundary Layers: Some Reflections on Forty Years of Research." *Journal of Sound and Vibration*, Vol. 190, pp. 299–315.

Bull, M. & Willis, J. (1961) "Some Results of Experimental Investigations of the Surface Pressure Field due to a Turbulent Boundary Layer." University of Southampton, Department of Aeronautics and Astronautics, Technical Report 199.

Cengel, Y. (2007) *Heat and Mass Transfer: A Practical Approach*. McGraw Hill.

Coles, D. & Hirst, E. (1968) "Computation of Turbulent Boundary Layers." In *AFOSR-IFP Stanford Conference*, volume 2.

Durst, F. & Tropea, C. (1981) "Turbulent, Backward-Facing Step Flows in Two-Dimensional Ducts and Channels." In *Proceedings of the Third International Symposium on Turbulent Shear Flows*, pages 18.1–18.5.

Eaton, J. & Johnston, J. (1980) "Turbulent Flow Reattachment: An Experimental Study of the Flow and Structure Behind a Backward-Facing Step." Department of Mechanical Engineering, Stanford University, Technical report.

Farabee, T. & Casarella, M. (1991) "Spectral Features of Wall Pressure Fluctuations Beneath Turbulent Boundary Layers." *Physics of Fluids*, Vol. 3, pp. 2410–2420.

Glauert, H. (1934) *Aerodynamic Theory.*, chapter Airplane Propellers, page 332 Dover.

Keith, W.; Hurdis, D.; & Abraham, B. (1992) "A Comparison of Turbulent Boundary Layer Wall-Pressure Spectra." *Transactions of the American Society of Mechanical Engineers, Journal of Fluids Engineering*, Vol. 114, pp. 338–347.

Kelley, N.; Jonkman, B.; & Scott, G. (2005) "The Impact of Coherent Turbulence on Wind Turbine Aeroelastic Response and Its Simulation." In *WindPower 2005*, Denver, Colorado.

Kim, J.; Kline, S.; & Johnston, J. (1978) "Investigation of Separation and Reattachment of a Turbulent Shear Layer: Flow over a Backward-Facing Step." Department of Mechanical Engineering, Stanford University, Technical report.

Klewicki, J.; Priyadarshana, P. A.; & Metzger, M. (2008) "Statistical Structure of the Fluctuating Wall Pressure and its In-Plane Gradients at High Reynolds Number." *Journal of Fluid Mechanics*, Vol. 609, pp. 195–220.

Kraichnan, R. (1956) "Pressure Fluctuations in Turbulent Flow Over a Flat Plate." *Journal of the Acoustical Society of America*, Vol. 28, pp. 378–390.

Le, H.; Moin, P.; & Kim, J. (1997) "Direct Numerical Simulation of Turbulent Flow Over a Backward-Facing Step." *Journal of Fluid Mechanics*, Vol. 330, pp. 349–374.

Lighthill, M. (1952) "On Sound Generated Aerodynamically. Part I: General Theory." *Proceedings of the Royal Society of London*, Vol. A211, pp. 564–587.

Panton, R. & Linebarger, J. (1974) "Wall Pressure Spectra Calculations for Equilibrium Boundary Layers." *Journal of Fluid Mechanics*, Vol. 65, pp. 261–287.

Prandtl, L. (1904) "Uöber Fluössigkeitsbewegung bei sehr kleiner Reibung." In *Third International Congress of Mathematics*.

Prandtl, L. (1925) "Uöber die ausgebildete Turbulenz." Z. Angew. Math. Mech., vol. 5, pp. 136-139.

Press, W. H.; Teukolsky, S.; Vetterling, W.; & Flannery, B. (1992) *Numerical Recipes in Fortran*. Cambridge University Press.

Reynolds, O. (1883) "On the Experimental Investigation of the Circumstances Which Determine Whether the Motion of Water Shall be Direct or Sinuous, and the Law of Resistance in Parallel Channels." *Philosophical Transactions of the Royal Society of London*, Vol. 174, pp. 935–982.

Serafini, J. (1963) "Wall Pressure Fluctuation and Pressure Velocity Correlations in Turbulent Boundary Layers." AGARD, Technical Report 453.

Sim, C.; Basu, S.; & Manuel, L. (2009) "The Influence of Stable Boundary Layer Flows on Wind Turbine Fatigue Loads." In *47th AIAA Aerospace Sciences Meeting Including the New Horizons Forum and Aerospace Exposition*, Orlando, Florida.

Willmarth, W. (1956) "Wall Pressure Fluctuations in a Turbulent Boundar Layer." *Journal of the Acoustical Society of America*, Vol. 28, pp. 1048–1053.

Willmarth, W. & Wooldridge, C. (1962) "Measurements of the Fluctuating Pressure at the Wall Beneath a Thick Turbulent Boundary Layer." *Journal of Fluid Mechanics*, Vol. 14, pp. 187–210.

Vita

David William Rich was born on October 20, 1986 in Flowood, Mississippi, to Neal and Cindy Rich. His father and mother worked as successful electrical and civil engineers respectively in the Jackson, Mississippi metro area where Rich spent his adolescent years.

After graduating high school at Madison Ridgeland Academy in May 2005, Rich attended the University of Mississippi with the aid of the Adler Engineering academic scholarship. While at Ole Miss, Rich was inducted into the national engineering honor society Tau Beta Pi, and earned a Bachelor of Science in Mechanical Engineering graduating magna cum laude in May 2009. During his undergraduate career Rich was active in his fraternity Sigma Nu and also served as a Lafayette County volunteer firefighter.

After deciding to return to school to pursue a graduate degree, Rich accepted a graduate research assistantship with the Aeroacoustics group at the National Center for Physical Acoustics at the University of Mississippi and began working there with Dr. Nathan Murray and Bernard Jansen in the fall of 2009. After graduation Rich plans to work for Dynetics in Huntsville, Alabama as an engineer working on acoustics projects for their signatures division.